NAVAL POSTGRADUATE SCHOOL

MONTEREY, CALIFORNIA

THESIS

INVESTIGATIONS OF NONLINEAR WAVES AND PARAMETRIC EXCITATION

by

William P. Jones

September 2005

Thesis Advisor:	Bruce C. Denardo
Co-Advisor:	Thomas Hofler

Approved for public release; distribution is unlimited

THIS PAGE INTENTIONALLY LEFT BLANK

REPORT DOCUMENTATION PAGE		Form Approved OMB No. 0704-0188
Public reporting burden for this collection of information is estimated to average 1 hour per response, including the time for reviewing instruction, searching existing data sources, gathering and maintaining the data needed, and completing and reviewing the collection of information. Send comments regarding this burden estimate or any other aspect of this collection of information, including suggestions for reducing this burden, to Washington headquarters Services, Directorate for Information Operations and Reports, 1215 Jefferson Davis Highway, Suite 1204, Arlington, VA 22202-4302, and to the Office of Management and Budget, Paperwork Reduction Project (0704-0188) Washington DC 20503.		
1. AGENCY USE ONLY ***(Leave blank)***	**2. REPORT DATE** September 2005	**3. REPORT TYPE AND DATES COVERED** Master's Thesis
4. TITLE AND SUBTITLE: Investigations of Nonlinear Waves and Parametric Excitation		**5. FUNDING NUMBERS**
6. AUTHOR(S) William P Jones		
7. PERFORMING ORGANIZATION NAME(S) AND ADDRESS(ES) Naval Postgraduate School Monterey, CA 93943-5000		**8. PERFORMING ORGANIZATION REPORT NUMBER**
9. SPONSORING /MONITORING AGENCY NAME(S) AND ADDRESS(ES) N/A		**10. SPONSORING/MONITORING AGENCY REPORT NUMBER** N/A
11. SUPPLEMENTARY NOTES The views expressed in this thesis are those of the author and do not reflect the official policy or position of the Department of Defense or the U.S. Government.		
12a. DISTRIBUTION / AVAILABILITY STATEMENT Approved for public release; distribution is unlimited.		**12b. DISTRIBUTION CODE**

13. ABSTRACT (maximum 200 words)

Nonlinearity in oscillations and waves can lead to dramatic and useful behavior. The course PH4459 at the Naval Postgraduate School was recently redesigned to extend its original subject of nonlinear acoustics to nonlinear oscillations and waves in general, with minimal prerequisites so that non-acoustics-tracked students can enroll in the course. Due to the unusual behavior and mathematical difficulty of nonlinear systems, lecture demonstrations are vital to the teaching of the course. The purpose of this thesis is to develop two new demonstrations for the course, and to improve an existing demonstration. In one of the new demonstrations, we investigate the generation and detection of high-amplitude waves on water to demonstrate the dependence of the wave speed upon amplitude. The experimental data agree with the theory. In the other new demonstration, we investigate a compression driver that exhibits a strong response at half the frequency of the drive. Data and the current scientific literature indicate that this behavior is due to parametric excitation of the deformation modes of the diaphragm assembly. Finally, we describe improvements to a torsional oscillator that is parametrically excited by modulation of its length. The improvements include a new motor, sturdier construction, and a new torsional strip.

14. SUBJECT TERMS Parametric excitation, torsional oscillator, gravity waves, and Parametric end fired array.			**15. NUMBER OF PAGES** 81
			16. PRICE CODE
17.SECURITY CLASSIFICATION OF REPORT Unclassified	**18.SECURITY CLASSIFICATION OF THIS PAGE** Unclassified	**19.SECURITY CLASSIFICATION OF ABSTRACT** Unclassified	**20. LIMITATION OF ABSTRACT** UL

NSN 7540-01-280-5500

Standard Form 298 (Rev. 2-89)
Prescribed by ANSI Std. 239-18

THIS PAGE INTENTIONALLY LEFT BLANK

Approved for public release; distribution is unlimited

INVESTIGATIONS OF NONLINEAR WAVES AND PARAMETRIC EXCITATION

William P. Jones
Ensign, United States Navy
B.S., United States Naval Academy, 2004

Submitted in partial fulfillment of the
requirements for the degree of

MASTER OF SCIENCE IN APPLIED PHYSICS

from the

NAVAL POSTGRADUATE SCHOOL
September 2005

Author: William P. Jones

Approved by: Bruce C. Denardo
Thesis Advisor

Thomas Hofler
Thesis Co-Advisor

James Luscombe
Chairman, Physics Department

THIS PAGE INTENTIONALLY LEFT BLANK

ABSTRACT

Nonlinearity in oscillations and waves can lead to dramatic and useful behavior. The course PH4459 at the Naval Postgraduate School was recently redesigned to extend its original subject of nonlinear acoustics to nonlinear oscillations and waves in general, with minimal prerequisites so that non-acoustics-tracked students can enroll in the course. Due to the unusual behavior and mathematical difficulty of nonlinear systems, lecture demonstrations are vital to the teaching of the course. The purpose of this thesis is to develop two new demonstrations for the course, and to improve an existing demonstration. In one of the new demonstrations, we investigate the generation and detection of high-amplitude waves on water to demonstrate the dependence of the wave speed upon amplitude. The experimental data agree with the theory. In the other new demonstration, we investigate a compression driver that exhibits a strong response at half the frequency of the drive. Data and the current scientific literature indicate that this behavior is due to parametric excitation of the deformation modes of the diaphragm assembly. Finally, we describe improvements to a torsional oscillator that is parametrically excited by modulation of its length. The improvements include a new motor, sturdier construction, and a new torsional strip.

THIS PAGE INTENTIONALLY LEFT BLANK

TABLE OF CONTENTS

THIS PAGE INTENTIONALLY LEFT BLANK

LIST OF FIGURES

LIST OF TABLES

THIS PAGE INTENTIONALLY LEFT BLANK

ACKNOWLEDGEMENTS

I would like to thank my family and loved ones for all the support they have given me. I would like to thank Professor Bruce Denardo for the patience and unwavering dedication to giving students the best possible learning experience. Thanks are also in order for Mr. Sam Barone and Mr. George Jaksha for their hard work in getting my demonstrations presentable.

THIS PAGE INTENTIONALLY LEFT BLANK

I. INTRODUCTION

Nonlinearity often plays an essential role in physical systems. Until the roughly the 1970s, physicists tended to be blind to this fact, and to focus only on linear systems, or on systems linearized about some state. Part of the reason for the neglect of nonlinearity was the attention paid to the development of relativity and quantum mechanics. However, the discovery of chaos abruptly changed physicists' attitudes, leading to investigations in a broad range of nonlinear phenomena in many fields. In the roughly 30 years that has elapsed, only a small part of the resultant wealth of knowledge is readily available to students other than those who specialization involves some area of nonlinear phenomena. With this in mind, Professors. Andrés Larraza and Bruce Denardo, in the Physics Department at the Naval Postgraduate School, recently redesigned the course PH4459, which was originally a course primarily in acoustic shock waves for acoustics-tracked students. The material was extended to cover nonlinear oscillations, nonlinear dispersive waves (such as ocean waves), and many other nonlinear acoustical phenomena in addition to shocks. In addition, the course is open to all students with minimal prerequisites.

Nonlinear behavior is often surprising, and is also conceptually challenging. In addition, analytical treatments are almost always difficult. Lecture demonstrations thus play a very important role in the teaching of PH4459. As a result of the attention over decades that the NPS Physics Department has given lecture demonstrations in all areas of physics, some nonlinear oscillation and wave demonstrations already exist, but many more are needed. These include some that are only concepts; that is, demonstrations that have not yet been developed at NPS or any other institution. The goal of this thesis is to develop several nonlinear oscillation and wave demonstrations for use in PH4459 and other courses.

We began with nonlinear capillary waves, which are short-wavelength surface waves on a liquid. Our hope was to develop two new demonstrations.

The first was to demonstrate that the wave speed increases with amplitude, for a fixed frequency. The second was to demonstrate that a wave can be created due to the nonlinear interaction of two waves at an angle. As discussed in Ch. II, however, difficulties with capillary waves forced us to reconsider our goals. The result, as discussed in Ch. III, is a demonstration that clearly shows the effect for gravity waves (longer-wavelength waves). Comparison of our data with the theory yielded good agreement.

Another project began as the construction of an acoustical parametric end-fired array in air. Due to substantial difficulties, this project was postponed for a future thesis student. However, while testing a compression driver, we found a very clear subharmonic at half the drive frequency of 20 kHz. We decided to pursue this interesting nonlinear effect. As detailed in Ch. IV, through collection and analysis of data, and comparison to the scientific literature, we show that this subharmonic is almost certainly due to parametric excitation of deformation modes of the diaphragm at high frequency, and parametric excitation of the fundamental mode of the compression driver at low frequency.

A previous student (Janssen, 2005) had built a length-modulated torsional oscillator as a demonstration of parametric excitation. However, many improvements need to be made before the system becomes suitable as a lecture demonstration apparatus. In Ch. V, we report on several major improvements that we have made. The most important improvements were a new motor, which was only decided upon after a detailed analysis, and a new torsional strip, which was only decided upon after extensive experimentation.

II. NONLINEAR TRAVELING CAPILLARY WAVES

In this chapter, we discuss nonlinear capillary waves and the construction of a variable capacitance wave height transducer to measure the height of capillary waves. The theory for this work is stated in Sec. A, the circuitry used in the sensor is addressed in Sec. B, the construction of the sensor is detailed in Sec. C, the calibration and experiments are discussed in Sec. D, the construction of the apparatus in Sec. E, and future work in Sec. F.

A. THEORY

Capillary waves are similar to gravity waves which will be addressed in chapter II, except surface tension supplies the restoring force rather than gravity. For deep capillary waves, which is usually the case considered because the shallow waves are strongly damped, the linear dispersion relationship is

$$\omega^2 = \sigma k^3 \ ,$$

where $\sigma = \alpha/\rho$, where α is the surface tension coefficient and ρ is the density of the liquid. The dispersion relationship for general surface waves on a liquid of depth h, where both gravity and capillarity act as restoring forces, is

$$\omega^2 = \left(gk + \sigma k^3 \right) \tanh(kh) \ .$$

For water, gravity and capillarity contribute equally ($gk = \sigma k^3$) when the wavelength is greater than 2 cm and the frequency is less than 13 Hz. (Landau and Lifshitz, 1959).

Our goal was to develop two capillary wave demonstrations. In the first demonstration, the velocity of plane capillary waves of definite frequency would be shown to increase with wave height amplitude. In the second demonstration, two plane capillary waves of the same frequency and amplitude would be launched in directions with included angle θ, and allowed to interact (Figure 1). To leading nonlinear order, capillary waves possess a cubic nonlinearity, which

implies that the interaction of two waves yields sum ($\mathbf{k}_1 + \mathbf{k}_2$) and difference ($\mathbf{k}_1 - \mathbf{k}_2$) waves. For capillary waves, a propagating sum wave occurs for $\theta = 90^o$, which is referred to as the *resonance* angle. The objective of the second demonstration was to observe a propagating sum wave as the angle θ was slowly varied through the resonance value.

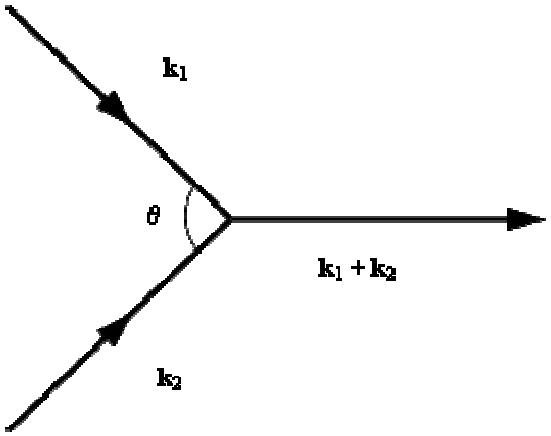

Figure 1. Nonlinear interaction of two waves. Sum (shown) and difference (not shown) waves are produced if the leading order nonlinearity is cubic.

B. WAVE SENSOR CIRCUITRY

The motivation of building this sensor was to find a convenient way to measure the height of the capillary waves using a two-wire probe as a variable capacitor. The water moving up the probe would cause a rise in capacitance and an increase in the output voltage. Eventually, there will be two sensors that will be placed in a one-dimensional wave channel to measure the wave velocity, and two or more sensors in a two-dimensional tank to measure the sum wave as two capillary waves nonlinearly interact.

The wave height sensor consists of different components. There are three chips that are used in the sensor and each of these chips has a specific purpose. The process of building the wave height sensor and inserting the chips will be discussed in Sec. C.

The first chip that is used in the wave height sensor is the CD4047BC chip which is shown in Figure 2. This is a low power monostable multivibrator, which is used in the wave height sensor as a square wave oscillator which provides the excitation for the sensor bridge.

The second chip is the INA110. This chip, which is shown in Figure 3, is called a Fast-Settling FET-Input Instrumentation Amplifier, and has the function of amplifying the difference signal at the output of the sensor bridge. The bridge is comprised of the wave probe capacitance and a fixed capacitor in one leg, and a pair of resistors with potentiometer ratio adjustment in the other leg. As the sensor capacitance increases from a nominal value so does the AC voltage difference of the bridge.

The third and final chip used in the transducer is the AD630 Balanced Modulator/ Demodulator chip. This chip, which is shown in Figure 4, acts as a single-channel lock-in amplifier to recover the signal from the background noise within the circuit. With this scheme, the frequency of the excitation signal being generated by the multivibrator chip is at least 100 times greater than the highest capillary wave frequency. At this excitation frequency it is easy to low-pass filter the output of the demodulator and effectively remove the excitation frequency component without attenuating the capillary wave frequencies.

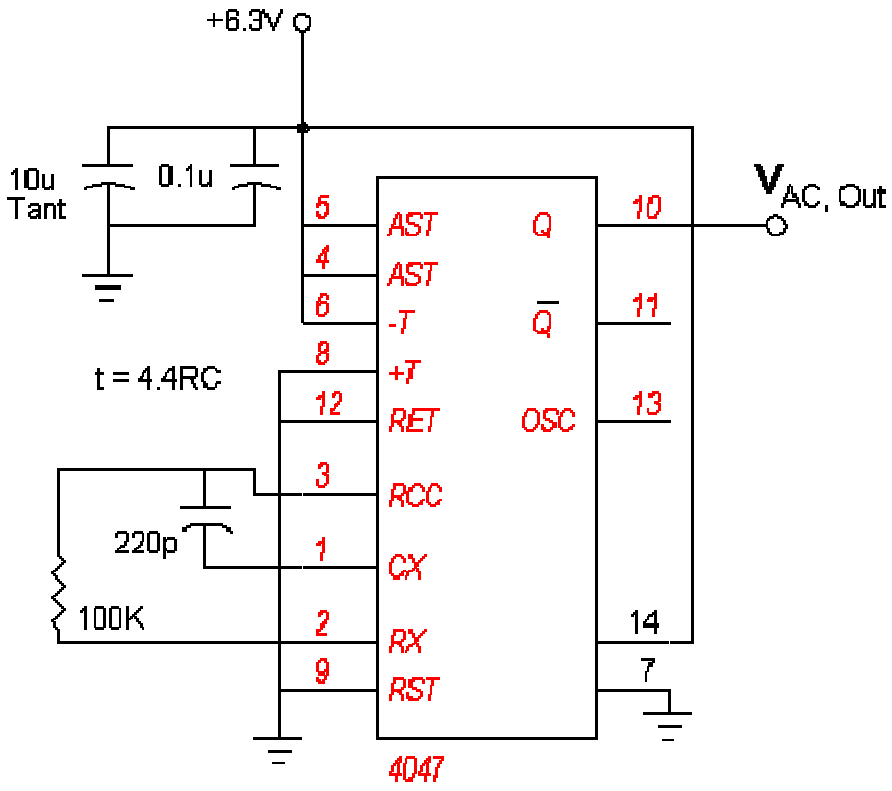

Figure 2. Square wave oscillator circuit.

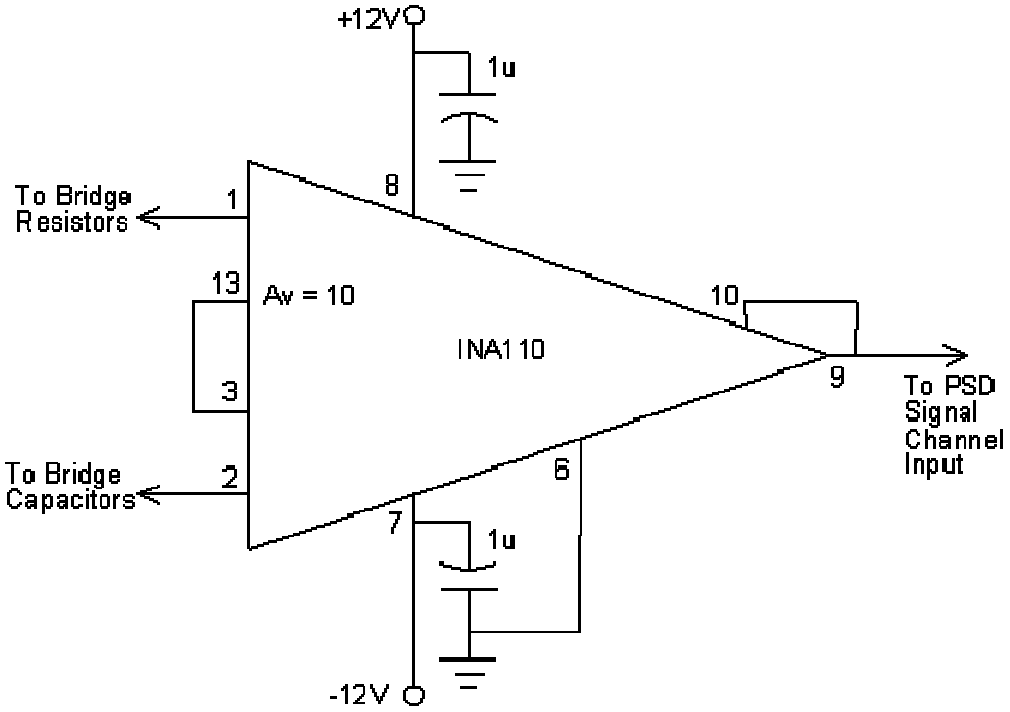

Figure 3. FET instrumentation amplifier.

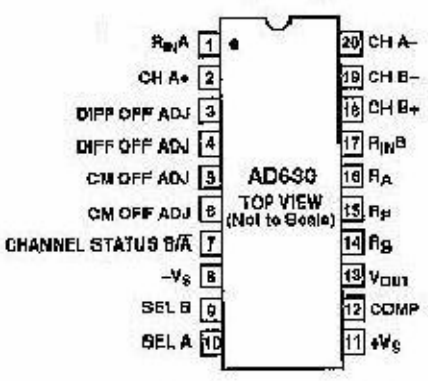

Figure 4. AD630 pin configuration.

C. SENSOR

There were several steps in building the wave height transducer. The first step consisted of building a power supply shown in Figure 5 and Figure 6. The power supply provides a 12 volt power source running down the two most outer rows of the circuit board. The next two outer rows are the ground supply. It was important to build the power supply first so that if problems did arise with the transducer the power supply would not be an issue. The power supply uses a CD4047BC chip discussed in section B and a low pass filter to strip off the DC.

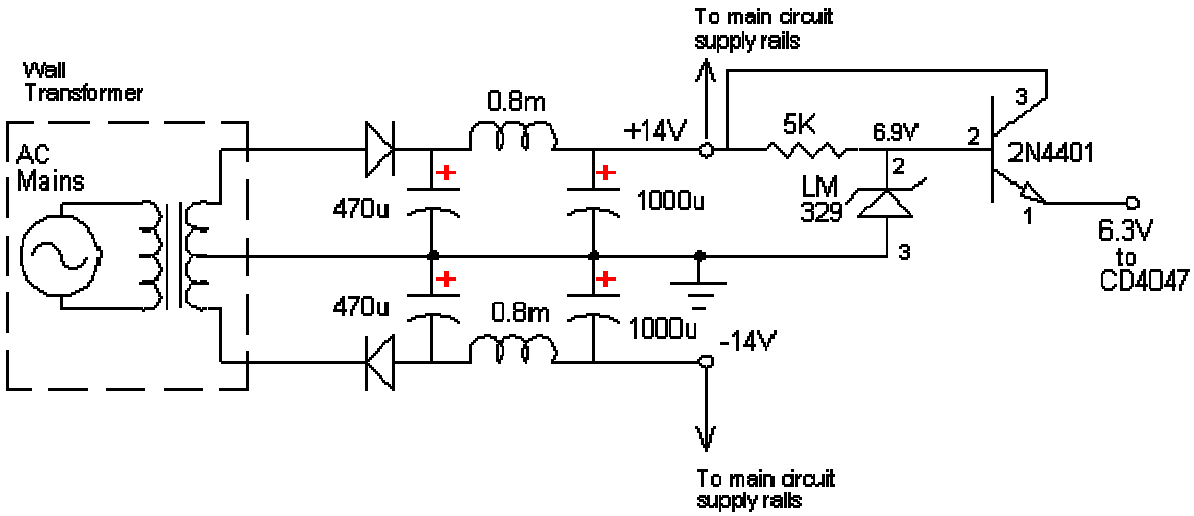

Figure 5. Power supply circuit designed by Dr. Thomas Hofler.

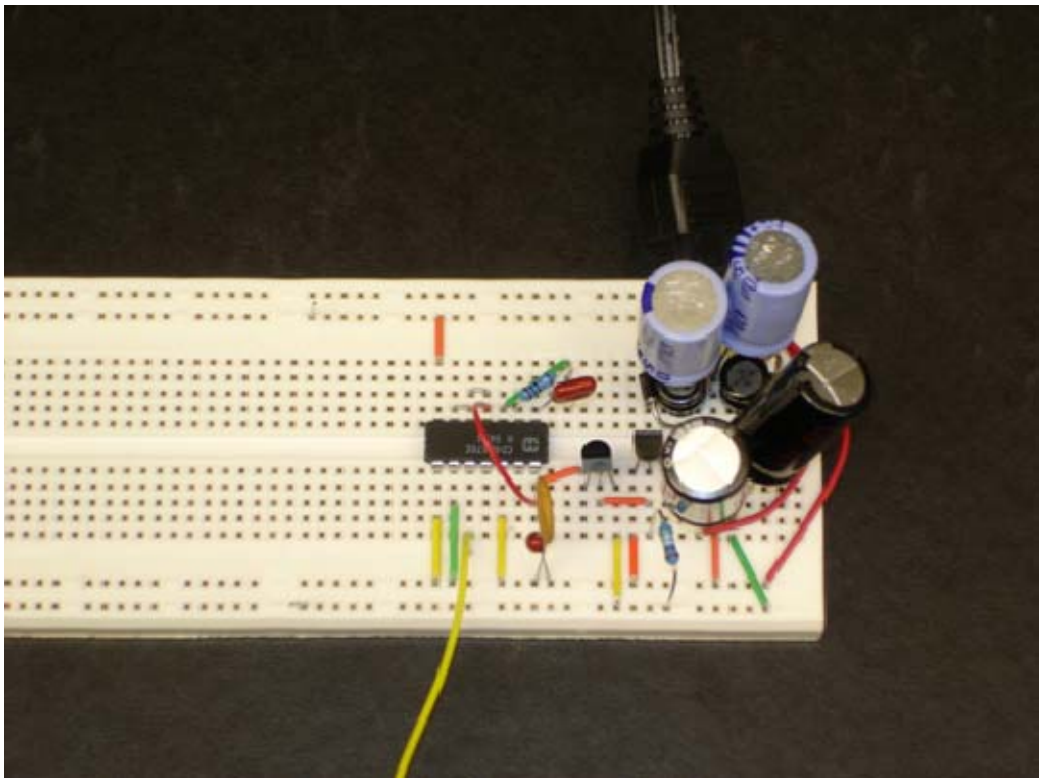

Figure 6. Power supply.

The next step in building the transducer consisted of building the AC capacitance bridge with a phase sensitive detector. The INA110 chip along with a series of capacitors and resistors was used to create this bridge. The most important parts of the design were the variable capacitor (the wave height sensor) and the variable resistor in which a heliopot was used. The wave height sensor consisted of two parallel wires which acted as a capacitor. The probe when submerged in water would cause an increase in capacitance which would cause an increase in the output voltage. This occurs because water has a higher dielectric constant than air. The heliopot or potentiometer was designed to zero out the output voltage at the initial submergence point. The probe was lowered into the water at a certain depth which would be the starting point for the measurements. At this starting point, an output voltage of zero was needed, and the heliopot provided the capability of doing this.

The third and final step in building the wave height transducer consisted of installing the AD630 Lock-in chip. An oscilloscope or multimeter is attached to output of this chip to measure the output voltage of the entire circuit. A simplified schematic of the entire circuit can be seen in Figure 7, and a picture of the actual circuit can be seen in figure 8.

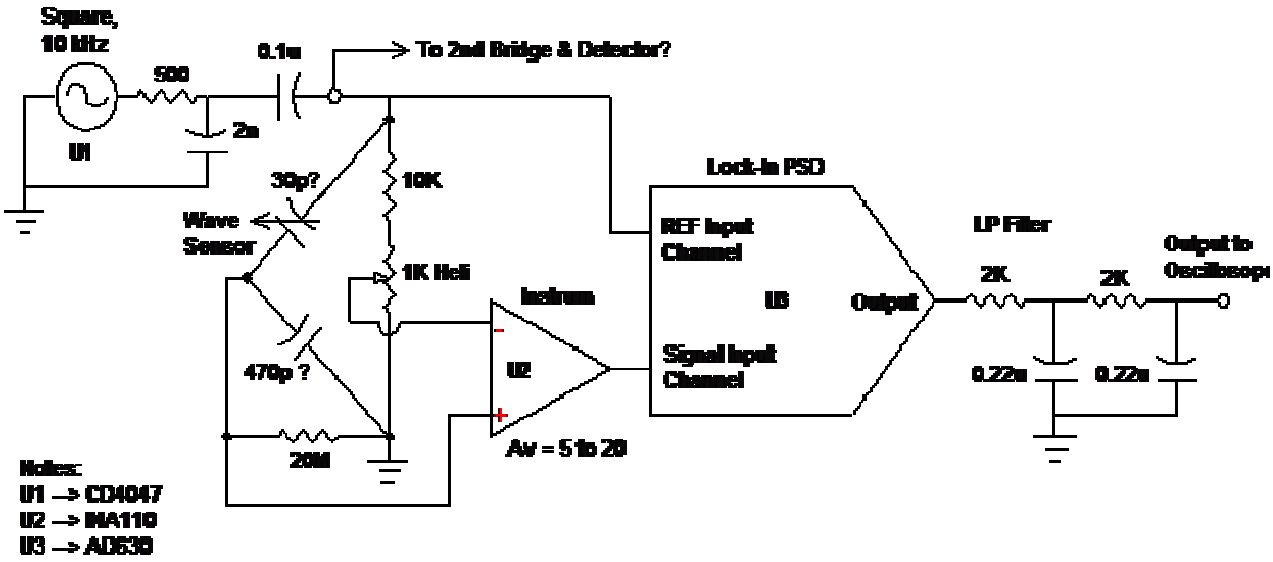

Figure 7. AC capacitance bridge with phase sensitive detector designed by Dr. Thomas Hofler (simplified schematic).

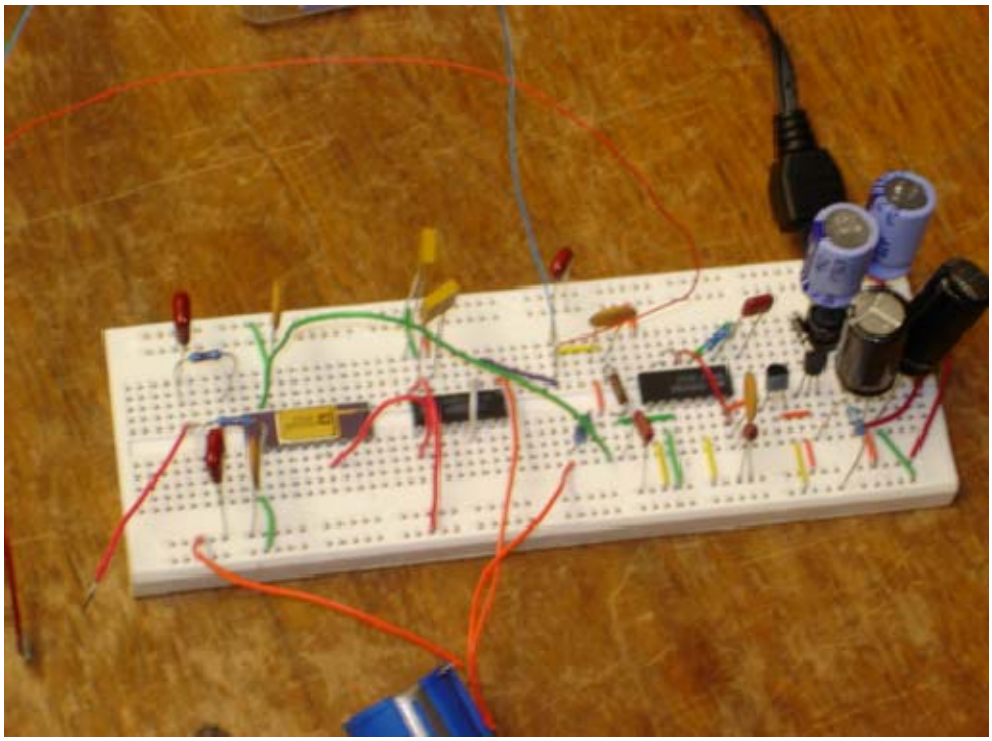

Figure 8. Wave height transducer with AC capacitance bridge.

D. CALIBRATION AND EXPERIMENTATION

There were three tests that we performed with this transducer. The first was to measure the frequency dependence of the capacitance with the transducer. The second was to do a static test to calibrate and get an idea of what values to expect from the transducer at certain depths or certain wave heights. The third step was to actually test the transducer using a shaker table to mimic wave heights that might be produced by the capillary wave demonstration.

Step one was accomplished by submerging the two-wire probe in a beaker of water and doing a frequency sweep from 500 Hz to 15 kHz on the impedance analyzer, so that we could have an accurate idea of what capacitance values to expect. Since water is a dielectric, as the depth in which the probe is submerged increases so will the capacitance. These first data runs were

performed to get an accurate idea of the frequency dependence of the capacitance. At the very low frequency of 600 Hz the capacitance is shown to be lower, but from the impedance analyzer data the capacitance values are almost uniform from that value up to 15 kHz. Figure 9 shows four frequencies that cover the spectrum at which the frequency sweep was done. The capacitance values for 4.92 kHz, 9.996 kHz, and 15 kHz are very close in value. The transducer will be operating at 10 kHz, so the frequency range tested provides an accurate estimate of the capacitance range. The expected capacitance ranges from 5 pF to about 100 pF. This was determined by submerging the probe in to a beaker of water and making several data runs.

The next step was to test the entire circuit under the same conditions using a multimeter to get the output voltages. Most often an oscilloscope will be used but since it was only a static measurement the multimeter sufficed. The data from the impedance analyzer expressed in figure 9 and the testing of the actual circuit expressed in figure 10 correlate very well. Both plots were linear, and when used to estimate the depth of the probe from a voltage or capacitance reading gave accurate measurements for other data runs.

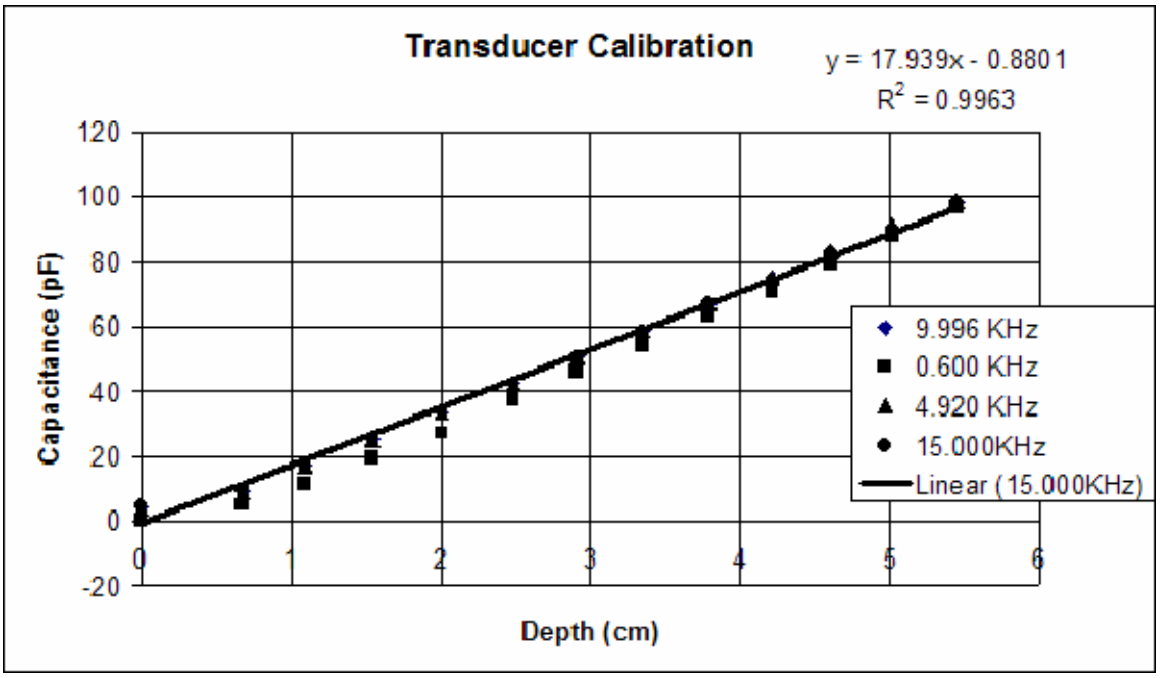

Figure 9. Impedance analyzer transducer calibration. Each frequency sweep is represented is represented by a different point.

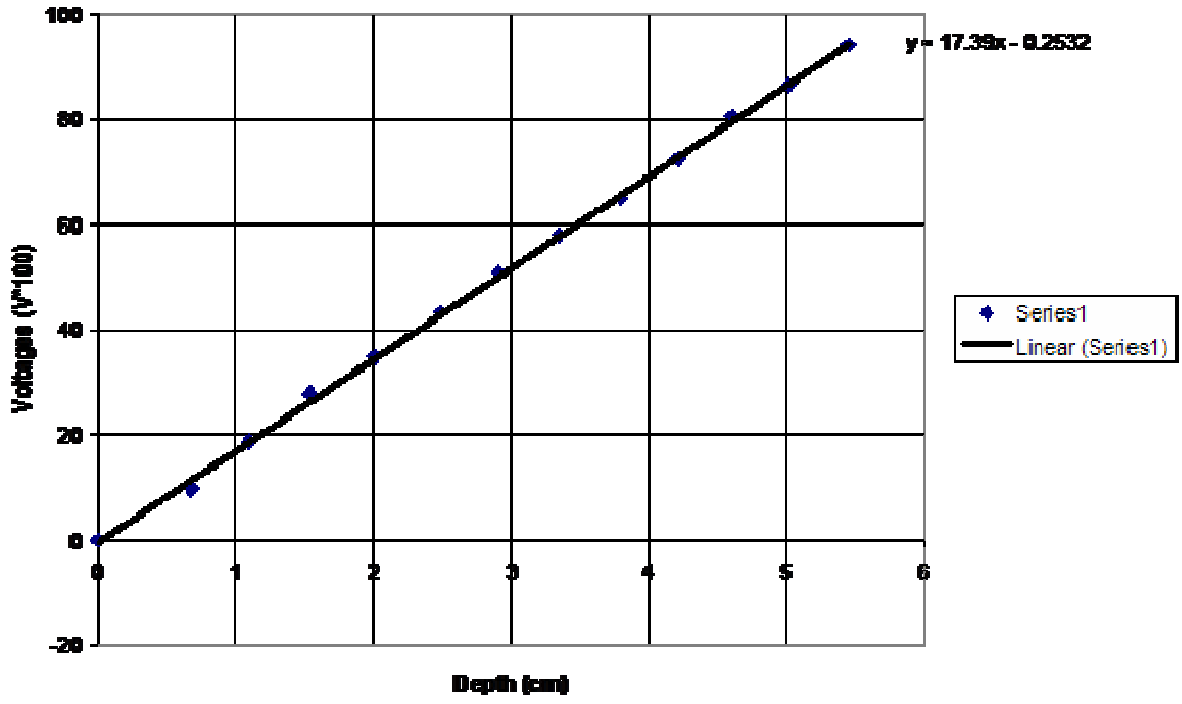

Figure 10. Static transducer calibration with bridge circuit.

The third and final calibration step was to perform a dynamic test of the wave height transducer. An APS shaker table was used to mimic the wave motion scenario for which the transducer was being built. The goal was to obtain an output voltage that would give an accurate measurement of the displacement of the shaker table which would have been checked by an accelerometer. I placed beaker of water on the shaker table, submerged the two-wire probe to its midpoint, and attached the accelerometer.

This test was unsuccessful due to the lack of sensitivity of the sensor, the displacement which the shaker table provided, and the meniscus sticking to the probe. These are a few of the reasons why the shaker table did not succeed as a good calibration test. The previous tests were all static and therefore did not have a problem with the meniscus because the depth changes were more pronounced than the displacement provided by the shaker table. Since the shaker table only provided for a vertical motion, the meniscus stuck to the probe worse than it would measuring traveling waves; however, this is the first of many problems with the design of this demonstration. The next step was to see what kind of values the probe gave for the capillary waves.

E. APPARATUS

The capillary wave apparatus shown in Figure 11 was comprised of a wave channel, an 8 inch driver, the wave height probe, and a wedge. The goal was to build a demonstration which would allow an audience to see the amplitude dependence of the velocity of capillary waves. The hope was then to expand the apparatus with the construction of a larger tank, a second driver, and a second probe, to demonstrate the nonlinear interaction of two capillary waves.

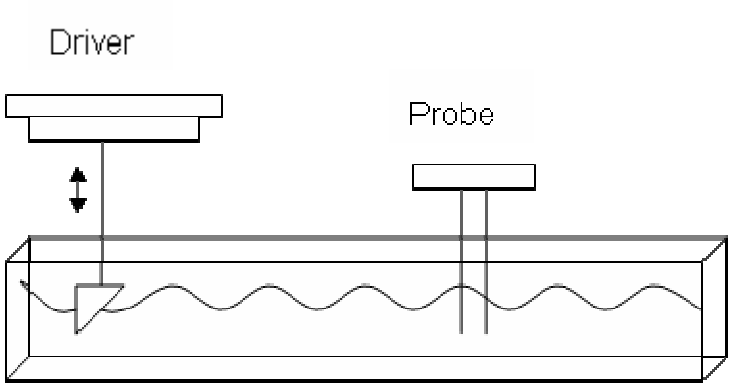

Figure 11. Capillary wave apparatus.

In attempting to build a working apparatus we went through several steps to try to produce the capillary waves. The first driver used was only 4 inches in diameter, and it could not withstand the drive voltage that was needed to get high amplitude capillary waves. The next step was to try a bigger driver that had a greater displacement and could handle the larger drive voltage. Even with a better driver it still proved difficult to produce the capillary waves. At the frequency range of 13 to 30 Hz, the wave forms being produced were very messy having almost no sinusoidal form.

Despite the difficulties with the wave height sensor, the production of this apparatus was halted by the inability to produce clean high amplitude capillary waves. We never actually measured any capillary waves with the wave height probe, but it seems from the dynamic test that unless the amplitude was much larger than predicted the sensitivity and the meniscus problems might make the sensor ineffective for this demonstration purpose. It might be possible to fix the meniscus problem by painting the probe wires with a hydrophilic coating such as an exterior latex paint. However, this was not tried since satisfactory capillary waves could not be produced.

We went down to a much lower frequency range to try and produce the waves, and in doing so we actually stumbled across the nonlinear effect of gravity waves which will be discussed in chapter II.

F. FUTURE WORK

This was an unsuccessful experiment. Due to the inability to produce the capillary waves the experiment was impossible to perform. The next step is to find some way in which these waves can be produced. Once that step is complete then finding a way to measure the waves is necessary. The sensor that was originally built worked well for later experiments with gravity waves, but it may not be a possibility for future work with capillary waves. Either a new probe that is more sensitive or using some sort of laser to measure the wave height would be ideal in performing this experiment.

III. NONLINEAR TRAVELING GRAVITY WAVES

In this chapter, we show that the speed of a finite amplitude surface wave on water depends upon the amplitude. This is a nonlinear effect. The theory for this work is stated in Sec. A, the methods of measurement in Sec. B and Sec. C, the experimental results in Sec. D, and future work in Sec. E.

A. THEORY OF NONLINEAR TRAVELING GRAVITY WAVES

We consider one-dimensional weakly nonlinear traveling waves on the surface of a deep liquid (Figure 12). The wavelength is assumed to be sufficiently large such that surface tension is negligible compared to gravity. For water, wavelengths greater than several centimeters satisfy this condition (Landau and Lifshitz, 1959).

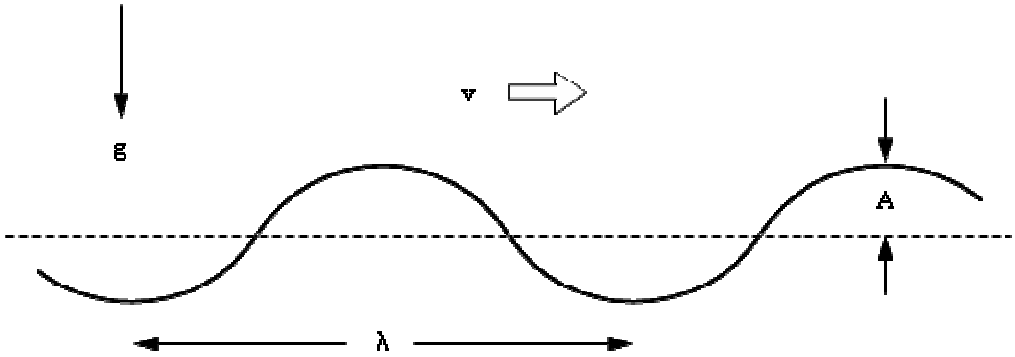

Figure 12. Geometry of a one-dimensional traveling gravity wave on a deep liquid. The peak amplitude is A, the wavelength is λ, and the wave moves with velocity v.

Linear theory (Landau and Lifshitz, 1959) yields the linear dispersion relationship

$$\omega^2 = gk \ , \qquad (3.A.1)$$

where $\omega = 2\pi f$ is the angular frequency of the wave (f is the frequency), and $k = 2\pi/\lambda$ is the wave number (λ is the wavelength). The linear wave (or *phase*) velocity is then

$$v_0 = \frac{\omega}{k} = \sqrt{\frac{g}{k}} = \frac{g}{\omega} , \qquad (3.A.2)$$

where we use the subscript "0" to denote the linear value as opposed to the weakly nonlinear value (see below).

A nonlinear calculation that is valid to leading order in kA << 1 yields the nonlinear dispersion relationship (Whitham, 1974)

$$\omega^2 = gk\left(1 + k^2A^2\right) , \qquad (3.A.3)$$

which was first derived by Stokes in 1847. Note that the quantity $kA = 2\pi A/\lambda$ is a measure of the maximum *steepness* of a wave. Because this quantity is assumed to be small, the square root of Eq. (3.A.3) is

$$\omega = \sqrt{gk}\left(1 + \frac{1}{2}k^2A^2\right) , \qquad (3.A.4)$$

to leading order in kA. The wave velocity $v = \omega/k$ is then

$$v = v_0\left(1 + \frac{1}{2}k^2A^2\right) , \qquad (3.A.5)$$

where we have substituted the expression (3.A.2) of the linear wave velocity.

In the experiment (Sec. 3.D), we deal with waves of fixed frequency $f = \omega/2\pi$. Because the nonlinear term in Eq. (3.A.5) is small, we use the linear dispersion relationship (3.A.1) to eliminate k in terms of f. The result is the theoretical wave velocity

$$v = v_0\left(1 + \frac{8\pi^4f^4}{g^2}A^2\right) , \qquad (3.A.6)$$

where

$$v_0 = \frac{g}{2\pi f} , \qquad (3.A.7)$$

from Eq. (3.A.2). A sketch of the relationship (3.A.6) is shown in Figure 13. The wave velocity increases quadratically with amplitude, which is valid to leading order in the amplitude. In Sec. 3.D, we compare experimental data to the theoretical expression (3.A.6) for the wave velocity as a function of wave height amplitude A for fixed frequency f.

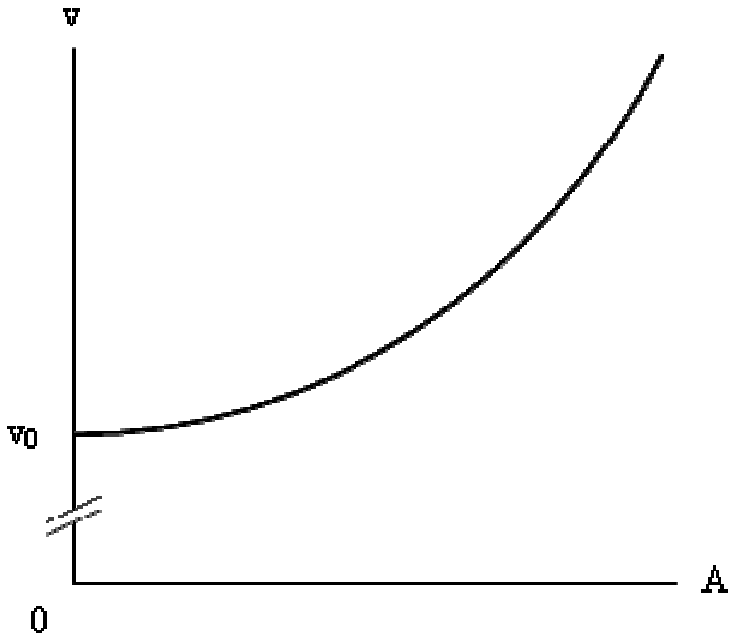

Figure 13. Sketch of the wave velocity v as a function of wave height amplitude A, for weakly nonlinear gravity waves on a deep liquid.

B. PHASE SHIFT METHOD

The dependence of the velocity of a wave upon the amplitude of the wave can be measured with a single probe. To accomplish this measurement, the instantaneous wave height is continuously measured with the probe at a fixed distance from a driver (Figure 14). The response voltage is sent to an oscilloscope that is triggered by the voltage source of the driver. As the drive amplitude and thus response amplitude are altered, a change in the wave velocity would be observed as a phase shift of the response (Figure 15). For waves whose velocity increases with amplitude, as predicted for gravity waves (Sec. 3.A), the peaks of the waveform on the scope occur at an earlier time, as shown in Figure 15.

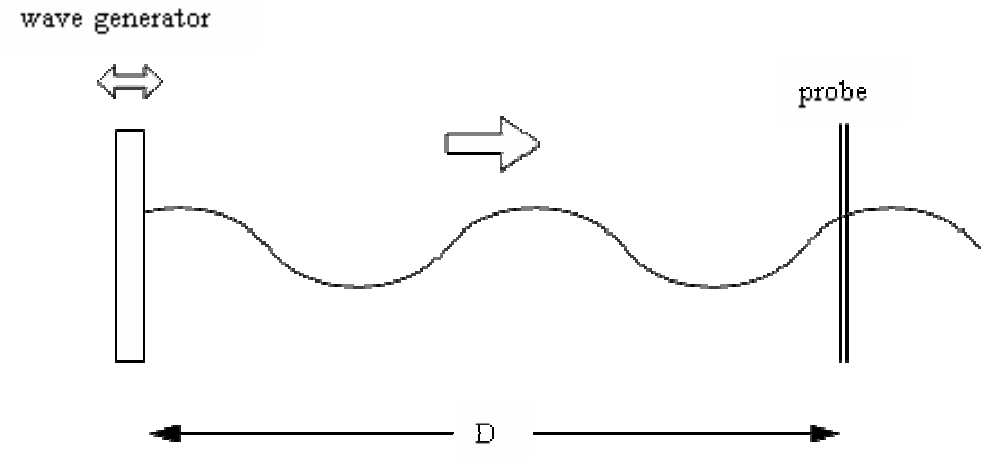

Figure 14. Arrangement to measure the dependence of the wave velocity on the amplitude of a wave. The drive frequency is held fixed as the amplitude of the drive is changed. The phase difference of the wave at the probe can be used to determine the shift in wave velocity.

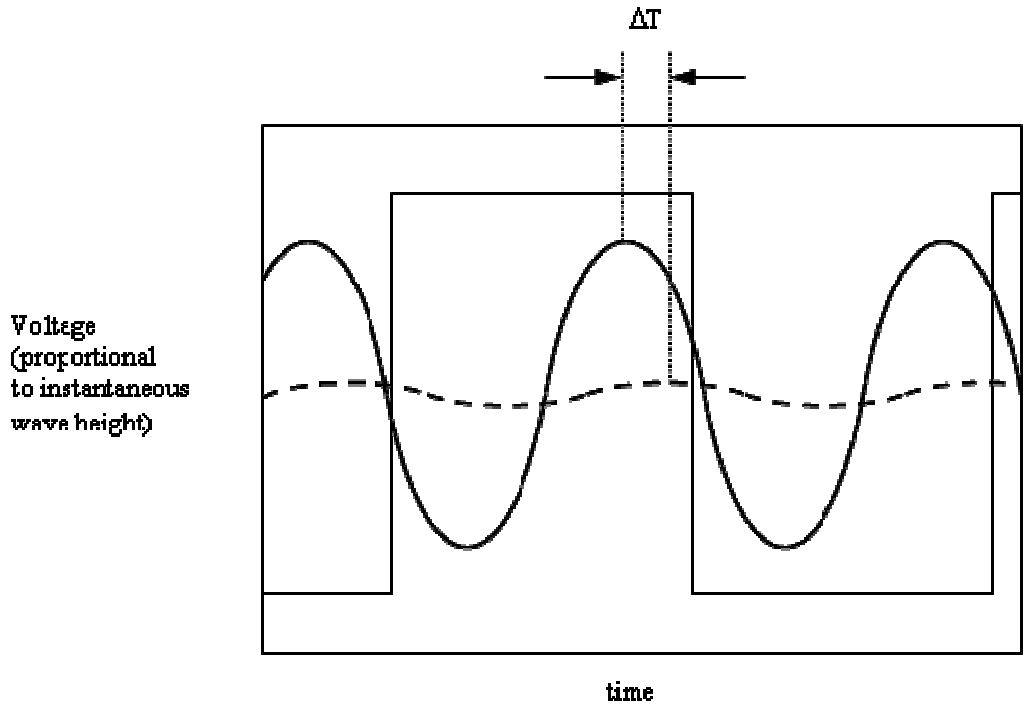

Figure 15. Representation of an oscilloscope display of the output of a wave height probe and a function generator. The square wave is from the driver voltage source (function generator), which is used as the trigger for the probe output. The dashed waveform is a small-amplitude (approximately linear) wave, and the solid waveform is a finite-amplitude waveform. The time interval ΔT is the time that a peak of the finite-amplitude wave occurs prior to the corresponding peak of the small-amplitude wave, which shows that the finite-amplitude wave has greater velocity.

The phase shifting toward earlier times is indeed what we observe in experiments. However, how do we know that the phase shifts are due to changes in the wave velocity and not, say, to a phase-dependence of the driver due to amplitude, or to some other effect? One way to resolve this issue is to compare the observed phase shifts with theoretical predictions based on changes in the wave velocity. Equivalently, we can use the experimentally measured phase shifts to determine the corresponding wave velocity (assuming that the phase shifts are caused by changes in the wave velocity). If agreement

occurs, then the phase shifts are almost certainly caused by the changes in wave velocity. We adopt this second comparison.

As in Sec. 3.A, we let v_0 refer to the wave velocity of a linear (infinitesimal amplitude) wave of frequency f, and v to the velocity of the finite-amplitude wave with the same frequency but with peak amplitude A. Suppose that the linear wave requires the time T to travel the distance D from the wave generator to the probe (refer to Figure 14):

$$v_0 = \frac{D}{T} , \qquad (3.B.1)$$

and that a finite-amplitude wave with the same frequency requires the time $T - \Delta T$ to travel the same distance:

$$v = \frac{D}{T - \Delta T} , \qquad (3.B.2)$$

The ratio of the velocities is then

$$\frac{v}{v_0} = \frac{T}{T - \Delta T} = \frac{1}{1 - \frac{\Delta T}{T}} = \frac{1}{1 - \frac{\Delta T}{D/v_0}} , \qquad (3.B.3)$$

or

$$v = \frac{v_0}{1 - v_0 \Delta T / D} . \qquad (3.B.4)$$

This expression allows us to determine the wave velocity from phase difference measurements ΔT, if the linear velocity v_0 is known. There are two alternatives for the determination of v_0. We can approximate this value from measurements of a small-amplitude wave, or we can use the theoretical linear wave velocity relationship (3.A.7). We adopt the latter procedure because it is simpler and more accurate. Furthermore, the linear theory will be experimentally tested by an independent and simpler method that is described in the next section.

C. WAVELENGTH METHOD

An alternative method to phase shift measurements (Sec. 3.B) is to directly measure the wave velocity by measuring the wavelength. The wave velocity, frequency, and wavelength for any wave of definite frequency are related by $v = \omega/k$, or

$$v = f\lambda \,, \qquad (3.C.1)$$

which is simply a statement that velocity equals distance divided by time. Because we deal with waves of fixed frequency, the fact that the wave velocity is predicted to increase with amplitude thus means that the wavelength should increase proportionally with amplitude. In the wavelength method, therefore, we directly measure the wavelength of the traveling gravity waves as a function of amplitude, and determine the wave velocity by simply multiplying the wavelength by the frequency, according to Eq. (3.C.1).

D. EXPERIMENTAL DATA AND COMPARISON TO THEORY

With the channel apparatus in Figure 16, we collected several sets of data. We used the same apparatus from the nonlinear capillary wave experiment. This apparatus was driven by an 8-inch loud speaker with a drive arm and a wedge as the wave generator. Another essential part of this experiment was the wave height sensor discussed in Chapter II and in section B of this chapter. This sensor gave us the ability to get the phase shift measurement of the wave form as the velocity increased. The wave tank was used for a prior demonstration purpose, and we were very fortunate to have such a precisely machined trough. The ruler was placed on the inside of the so that a proper scaling could be applied to the measurements taken by photo which will be discussed later in this section. Any improvement to this design and future work that should be carried out will be left for discussion in section E.

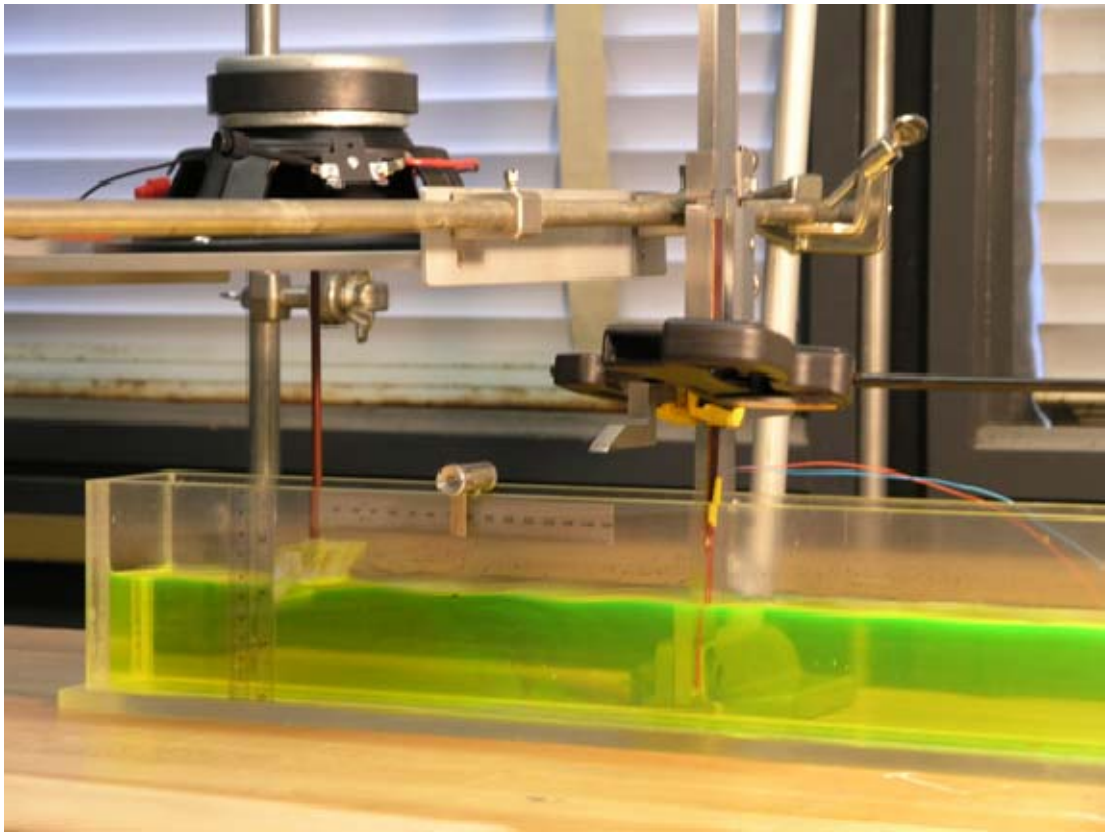

Figure 16. Gravity wave apparatus.

As stated in sections B and C, we used the wavelength method and the phase shift method to analyze the data in which we collected. Before we can discuss that outcome of the experimental data, we must first discuss how we collected the data and the uncertainties in our data. We will then show the final outcome of our experiment.

Using a multimeter, an Infinium oscilloscope, a power amp, a function generator, and a filter, we were able to collect our data. We were driving at a constant frequency of 5 Hz and would increase the amplitude of the waveform by a voltage increase to the wave generator. Before actually collecting data we would increase the drive voltage across the wave generator to its maximum. This was done to wet the probe, so that the lower amplitude waves would be picked up by the probe. After the wetting of the probe we would decrease the drive voltage to the lowest possible amount so that a sinusoidal wave was still visible on the oscilloscope. From this point we would then record the drive voltage value, the starting point to take the phase shift measurements, and four photos so that the amplitude value and wavelength value could be measured. The drive voltage was then increased and recorded. At each of these following drive voltages, the phase shift data was collected from the Infinium and photographs were taken to allow for the wavelength and amplitude measurements.

The data taken from the Infinium oscilloscope was a direct measurement and did not involve much effort other than using the marker feature on the scope itself. The wavelength and amplitude measurements did however take a bit more effort in measuring. Seen in Figure 17 is a series of photographs in which amplitude and wavelength measurements were taken. Each of these photographs was taken with an Olympus 8 megapixel camera. Putting fluorescein in the water allowed for a better contrast and easier measuring. The ruler that is attached to the side of the acrylic tank also allowed for the proper scaling in measuring the waveforms. Due to the small amplitude and the difficulties in measuring these values, we measured the peak-to-peak amplitude

rather than that of the peak amplitude. The waves also decayed so rapidly that we measured half the wavelength and multiplied by two so that the values would be more accurate. After measuring the data from our photographs and matching the phase shift measurement with the proper amplitude measured from the photos we then plotted our data.

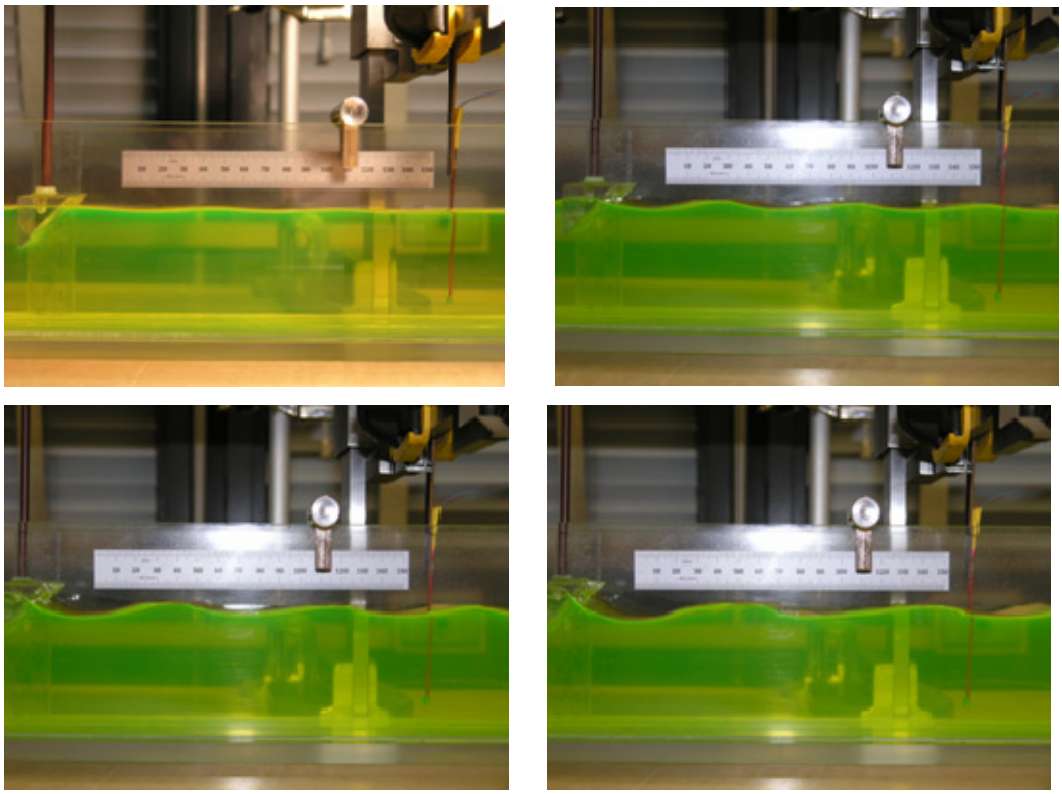

Figure 17. Waveform photographs from which amplitude and wavelength measurements were taken.

In all experimental work there are uncertainties that must be taken into account. Our experiment had several uncertainties, and we must address these so that we can determine the error bars that need to be inserted into the graph. To obtain an uncertainty from the data collection itself we would have to have taken many data runs, and since that was not feasible we will assign uncertainties. For the amplitude measurement, the uncertainty is just a direct assignment, but for the velocities for the wavelength and the phase shift method we must calculate the effects of the uncertainties on the velocity values. In the wavelength measurement the uncertainty is determined as follows:

$$v = f\lambda, \tag{3.D.1}$$

$$\delta v = \lambda\delta f + f\delta\lambda, \tag{3.D.2}$$

where δf can be assumed to be zero. Hence,

$$\delta v = f\delta\lambda = 2f\delta\left(\lambda/2\right) \tag{3.D.3}$$

is the final uncertainty equation since our measurements were of the half wavelength. The uncertainty value for $\delta\left(\lambda/2\right)$ is 3 mm.

For the phase shift method the uncertainty is determined as follows:

$$v = \frac{v_0}{1 - v_0\Delta T/D}, \tag{3.D.4}$$

$$\delta v = \frac{v_0}{(1 - v_0\Delta T/D)^2}\left[\frac{v_0\delta(\Delta T)}{D} - \frac{v_0\Delta T}{D^2}\delta D\right], \tag{3.D.5}$$

where δD can be ignored since its effects are negligible compared to that of $\delta(\Delta T)$. The final equation used for the uncertainty is then

$$\delta v = v^2\left[\frac{\delta(\Delta T)}{D}\right], \tag{3.D.6}$$

where we assign a $\delta(\Delta T)$ value of 30 ms.

In terms of the peak-to-peak amplitude $A_{pp} = 2A$, the relative wave velocity (3.A.6) is

$$v = v_0\left(1 + \frac{2\pi^4 f^4}{g^2}A_{pp}^2\right), \qquad (3.D.7)$$

which is the curve in Figure 18. The value of the linear wave velocity v_0 is determined from the relationship (3.A.7). Also in Figure 18 we have plotted our experimental results. From the graph, we can see that the data from the wavelength method agrees with the theory, except for the point corresponding to the greatest amplitude. The data from the phase method matches to the theoretical curve at the lower amplitudes; however, it increases faster than the theoretical for the higher amplitude values. The discrepancy is due to the significant decay of the amplitude of a wave. When we applied the wavelength method to an entire wavelength rather than one-half wavelength, the phase and wavelength methods yielded approximately the same wave velocities. The qualitative effect (a wave having greater velocity at greater amplitude) can be observed as a demonstration, but to get a precise data analysis of this process several improvements need to be made. Each of these improvements will be addressed in section E

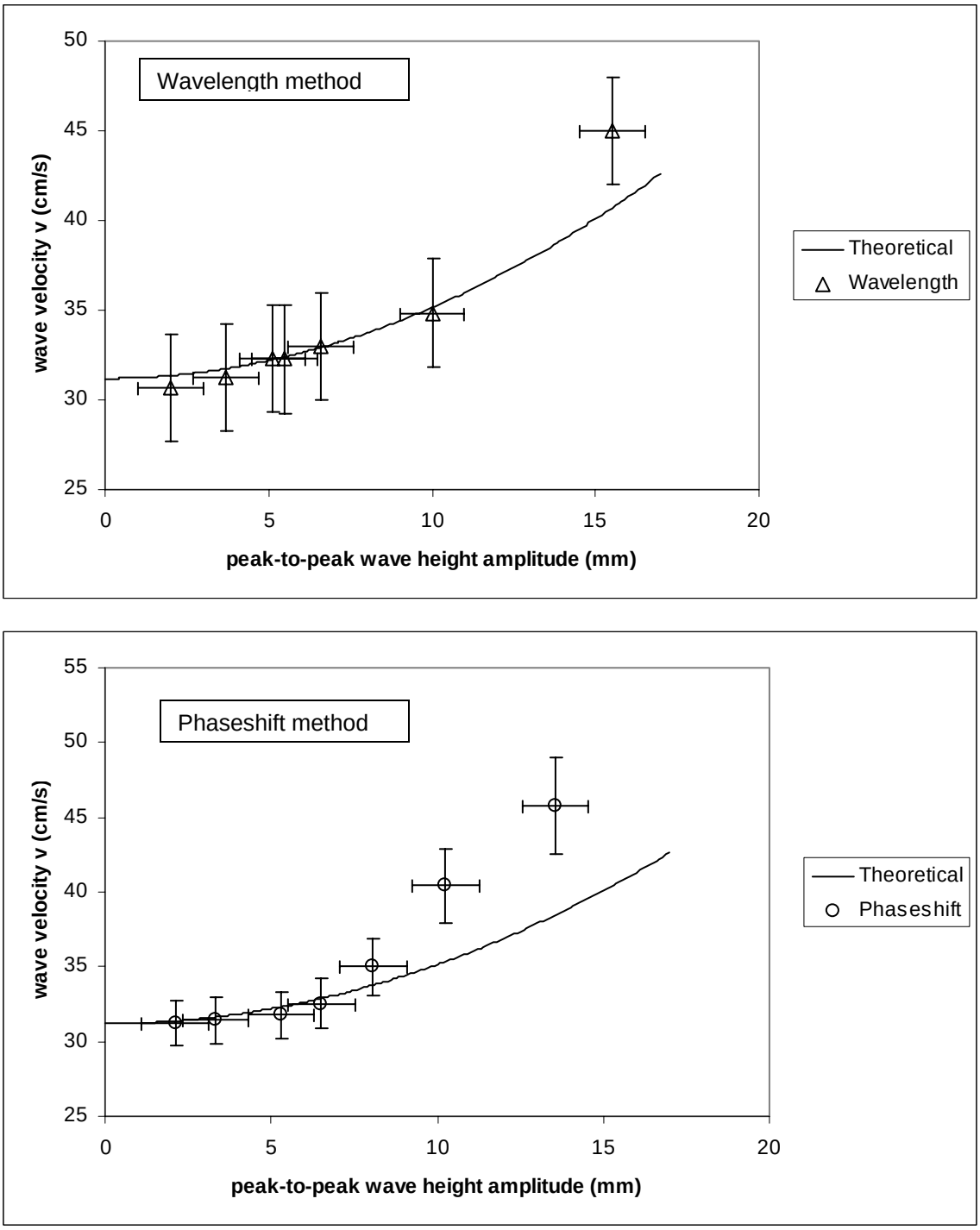

Figure 18. Wave velocity of 5.0 Hz gravity waves as a function of wave height amplitude. The curve is theoretical. The circles are experimental values from the phase shift method, which uses the theoretical linear value v_0 of the wave velocity for infinitesimal amplitude. The triangles are experimental values from the wavelength method.

E. FUTURE WORK

The traveling gravity wave apparatus provides an opportunity to study nonlinear gravity waves. This demonstration has potential, but needs work before it is ready for the classroom. There are several improvements that need to be made. The first improvement is the construction of two wave height probes that will provide the demonstrator both phase shift and amplitude data. In our experiment thus far we have been working with one probe, and because of this have had to use the theoretical linear wave velocity for our phase shift measurements. Using two probes will give us the $v_0 = D/T$ value that we assumed to be $v_0 = g/\omega$ in our measurements. The second improvement is a new wave generator. The idea for this new wave maker is to construct a paddle seen in Figure 19 that will have the drive horizontal rather than vertical as seen in Figure 16. This will allow the probes to be placed closer than before so that the initial waves can be measured before decay. The final improvement would be to make the wave tank longer. It is possible that some of the interference at higher amplitudes was due to reflections from the other end of the tank. If some type of beaching or other damping method was applied at the end of the tank, it could possibly help get data at higher amplitudes. These are the improvement that must be made to tank the next step in making this demonstration classroom ready.

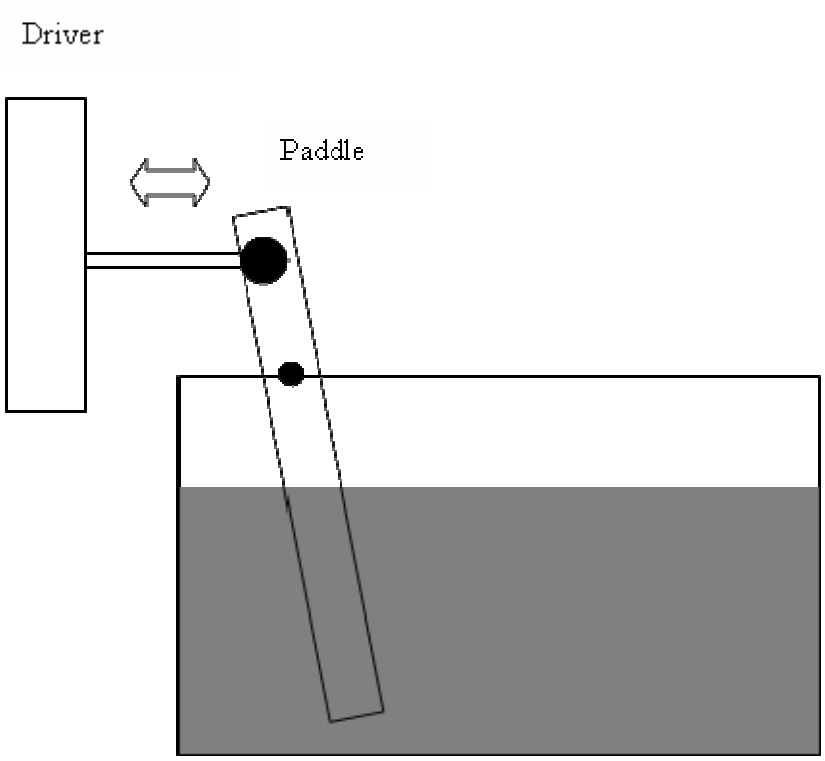

Figure 19. Drawing of prospective wave generator where the circles represent the pivot points on the paddle.

THIS PAGE INTENTIONALLY LEFT BLANK

IV. PARAMETRIC INSTABILITY OF A COMPRESSION DRIVER

One of the projects that we began for this thesis was the construction of a parametric end-fired array to operate in air. Due to various difficulties, we decided to postpone this project for a future thesis. However, while experimenting with different drivers, we observed a very clear f/2 subharmonic response when a compression driver was driven at a frequency of f = 20 kHz. In this chapter, we describe a lecture demonstration, experimental results, and scientific literature regarding this phenomenon.

A. BACKGROUND

If a parameter of an oscillatory system is modulated by an external source, it is possible to excite oscillations. This *parametric excitation* is most readily achieved when the drive frequency is twice the natural frequency of a mode of the system, and only occurs when the drive amplitude exceeds a threshold that is dictated by the dissipation of the system. A simple example is a pendulum whose length is modulated by hand. This can be accomplished with a weight attached to a string, where the string passes through an eyelet formed by the index finger and thumb of one hand. The other hand pulls the string horizontally back and forth. If the drive frequency is approximately twice the pendulum frequency, and the drive amplitude is sufficiently large, parametric excitation will occur.

The source need not be external to the oscillator. Due to a quadratic nonlinear coupling of modes, an excited mode can parametrically excite another mode if the frequency of the first mode is approximately twice the frequency of the second, and if the threshold condition is met. (If the coupling is cubic, it is readily shown that the frequencies of the modes should be equal.) This *internal* parametric excitation is sometimes referred to as *autoparametric excitation*. If the first mode is not driven externally, its amplitude must decrease by energy

conservation, and so this behavior is referred to as a *parametric instability*. When the first mode is externally driven, the amplitudes of both modes typically remains constant. This steady-state situation is often called *subharmonic generation* (f/2 in this case, where f is the drive frequency). However, it should be noted that *f/2 subharmonic generation need not be due to parametric excitation*. An example is a driven pendulum, which is well known to exhibit a period-doubling route to chaos. A response at f/2 can occur even though there is no mode at or near that frequency.

Perhaps the simplest and most common parametric instability can occur when a mass suspended by a spring is set into vertical oscillation. If the frequency is approximately twice the pendulum frequency, the pendulum mode is parametrically excited, which causes the amplitude of the vertical mode to decrease. A nonlinear beating motion then occurs. The reason for the parametric instability in this system is clear: the vertical mode essentially acts to replace the external source in the above example of a pendulum whose length is modulated.

A system of two coupled nonlinear oscillators exhibits a dramatic parametric instability that is not easily explained (Denardo et al., 1999). Figure 20 shows an example of two identical coupled pendulums. The symmetric mode, in which both pendulums oscillate in phase with the same amplitude, is unstable if the amplitude is above a threshold value.

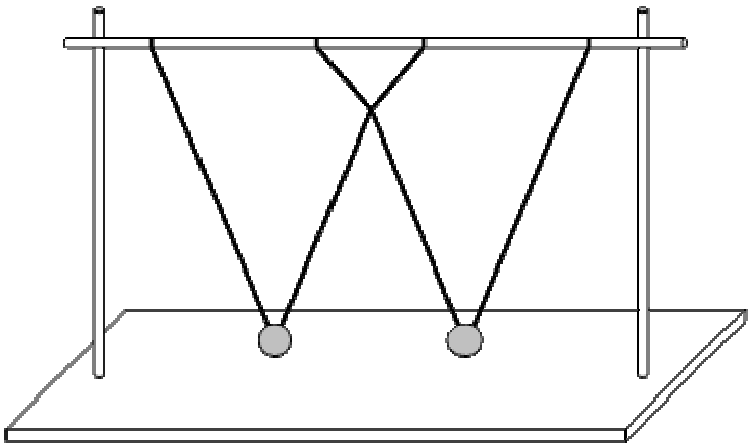

Figure 20. Coupled pendulum apparatus. The symmetric mode, in which both pendulums oscillate in phase with the same amplitude, is unstable if the amplitude exceeds a threshold value. This behavior is an example of a parametric instability.

B. DEMONSTRATION

A simple lecture demonstration of subharmonic generation can be accomplished with a compression driver (Figure 21). The compression driver is driven at an ultrasonic frequency so that the audience cannot hear the tone. We drive a JBL 2450 model with no horn at f = 20 kHz. The presence of the tone is detected by a microphone that is connected to a spectrum analyzer. The display can be projected onto a screen for clear viewing. As the drive amplitude is slowly increased from zero, the peak in the spectrum slowly grows. At approximately 1.0 V_{rms}, a response abruptly appears at half the drive frequency (f/2 = 10 kHz), and reaches a significant steady-state value. This subharmonic generation is heard by the audience, and is also observed on the spectrum analyzer (Figure 22). After discovering this demonstration, we found that Bolaños (2005) had recently pointed it out.

In this system, as in many systems, the presence of a subharmonic is undesirable. A loudspeaker or compression driver, especially in music

reproduction and sound reinforcement, is expected to accurately convert an electrical signal to an acoustical one. The clear presence of the subharmonic tone when the fundamental tone cannot be heard is a dramatic demonstration of a limitation of the driver.

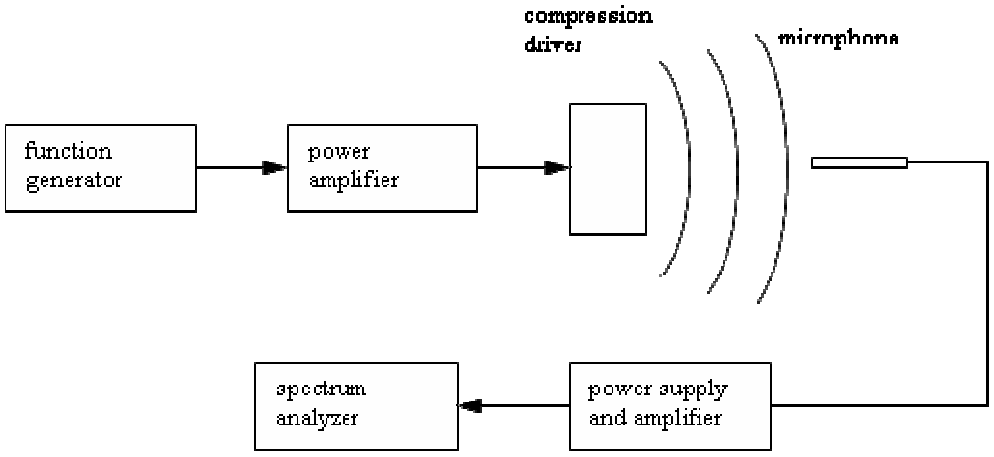

Figure 21. Schematic diagram of a demonstration of an f/2 subharmonic from a compression driver. The function generator is set to f = 20 kHz. As the amplitude of the drive signal to the compression driver is slowly increased, a 10 kHz tone is eventually abruptly heard. The f and f/2 responses are observed on the spectrum analyzer.

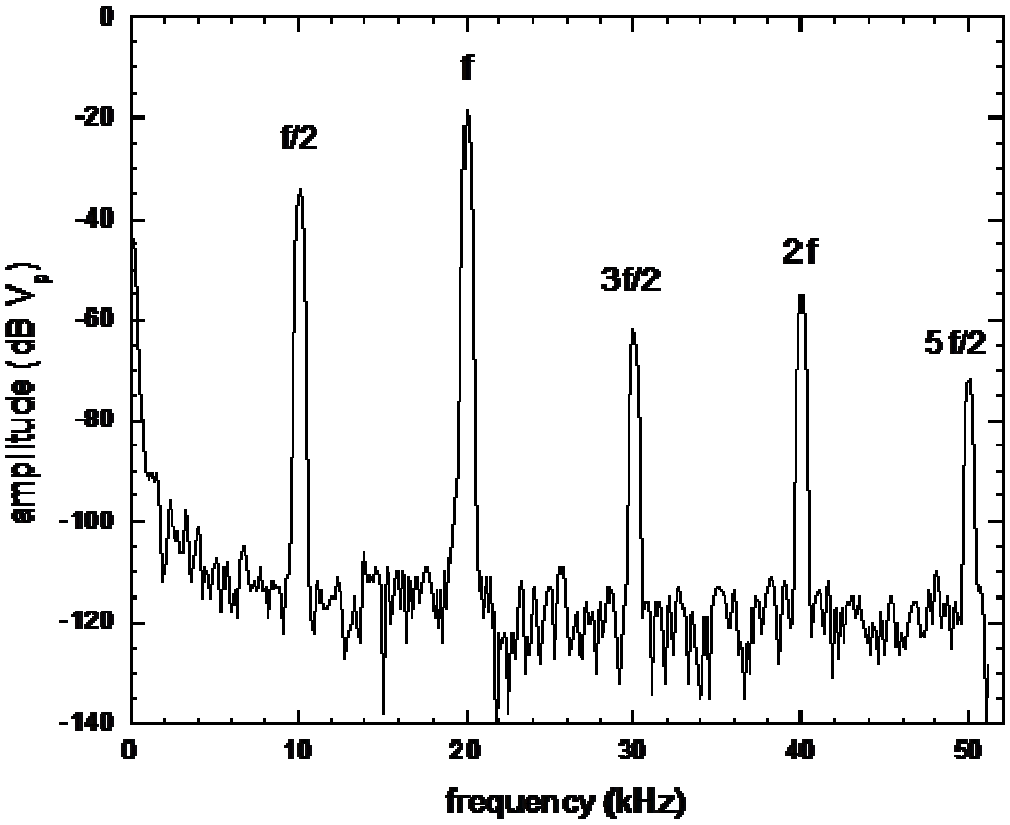

Figure 22. Spectrum of the sound from a JBL 2450 compression driver that is driven at frequency f = 20 kHz. The drive amplitude is 1.0 V_{rms}, which is slightly above the threshold for the appearance of the signal at f/2 = 10 kHz.

C. EXPERIMENTAL DATA

The main question regarding the response of a compression driver at half the drive frequency is whether or not this subharmonic is due to parametric excitation of a mode, and, if so, what mode is being parametrically excited. We pursued two paths of inquiry to answer this question: gathering data from our system (Sec. B), and studying the relevant scientific literature. The literature is discussed in the next section (Sec. D).

A remarkable feature of the subharmonic response in our system is that it arises abruptly as the drive amplitude is slowly increased. This is important for several reasons. First, it allows for precise experimental determination of the drive amplitude threshold (minimum value) for subharmonic generation. Second, an abrupt threshold is a well-known behavior of parametric excitation, so parametric excitation is not ruled out as the cause of subharmonic generation in our system. The quantitative meaning of “abrupt” is that the steady-state amplitude of the subharmonic as a function of drive amplitude has infinite slope at threshold. Figure 23 shows the subharmonic amplitude measured with a microphone 20 cm from the mouth of the compression driver. The amplitude is measured as a function of the drive voltage to the driver, for a constant drive frequency of 20 kHz. The subharmonic amplitude indeed appears to extrapolate to an infinite slope at threshold.

An obvious question is what drive frequencies other than f = 20 kHz does the f/2 subharmonic occur in our system. We focused our attention on the range f = 14 to 26 kHz. Subharmonic response was found for drive frequencies outside this range, but only at drive voltages that were near the limit of the driver, which is roughly 15 V_{rms}. An exception occurred at 1.0 kHz, where we observed f/2 subharmonic generation at about 4.0 V_{rms}. At each frequency incremented by 1.0 kHz, we determined the threshold drive amplitude at which the subharmonic occurred. If a mode is being parametrically excited, the plot of threshold drive amplitude vs. drive frequency should be approximately a hyperbola in which the

minimum is at twice the natural frequency of the mode being parametrically excited. Our data had the rough appearance of a hyperbola, but the data were not steadily decreasing and then steadily increasing as the frequency increased. Several small crests and troughs were indicated, but the density of points was insufficient to establish this. We thus decreased our frequency increment to 0.5 kHz, but this did not lead to smoothly-varying data. We then decreased the increment a third time, the results of which are shown in the top graph of Figure 24. Surprisingly, the data are still not smoothly-varying, even though the frequency increment is only 0.2 kHz.

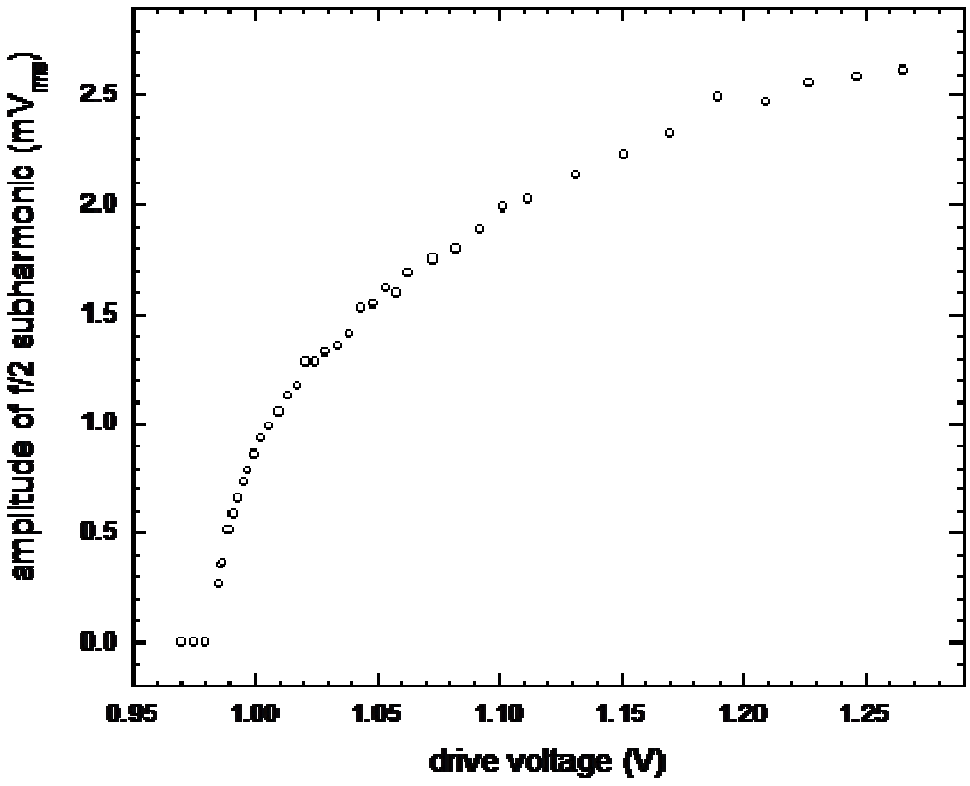

Figure 23. Subharmonic (f/2) response as a function of drive amplitude for a constant drive frequency of f = 20 kHz. The response rises abruptly at the drive amplitude threshold of 0.982 V_{rms}.

We refer to the response at the frequency of the drive as the *primary* response. If the primary response were parametrically exciting the subharmonic, the amplitude of the subharmonic would be an increasing function of the amplitude of the primary response. Because we were concerned that the primary amplitude may not be constant for different frequencies, we also gathered data on the relative amplitude of the primary response, from the microphone output. These data are shown in the bottom graph of Figure 24. The amplitude is indeed not constant, but substantially varies. Furthermore, there is a strong correlation between the variations of the threshold data and the primary response data below 20 kHz. This prompted us to normalize the threshold amplitude data to the primary amplitude, as a more accurate representation of the threshold of the subharmonic. Figure 25 shows the ratio of the threshold amplitude to the primary amplitude. The result is that the data vary more smoothly, and genuine minima are now apparent. It should be noted that the minima are much more pronounced on a linear scale, rather than a logarithmic scale which was used in order to clearly show all of the data. The minima are important because each may correspond to parametric excitation of a different mode. We explore this possibility further in the next section (Sec. D).

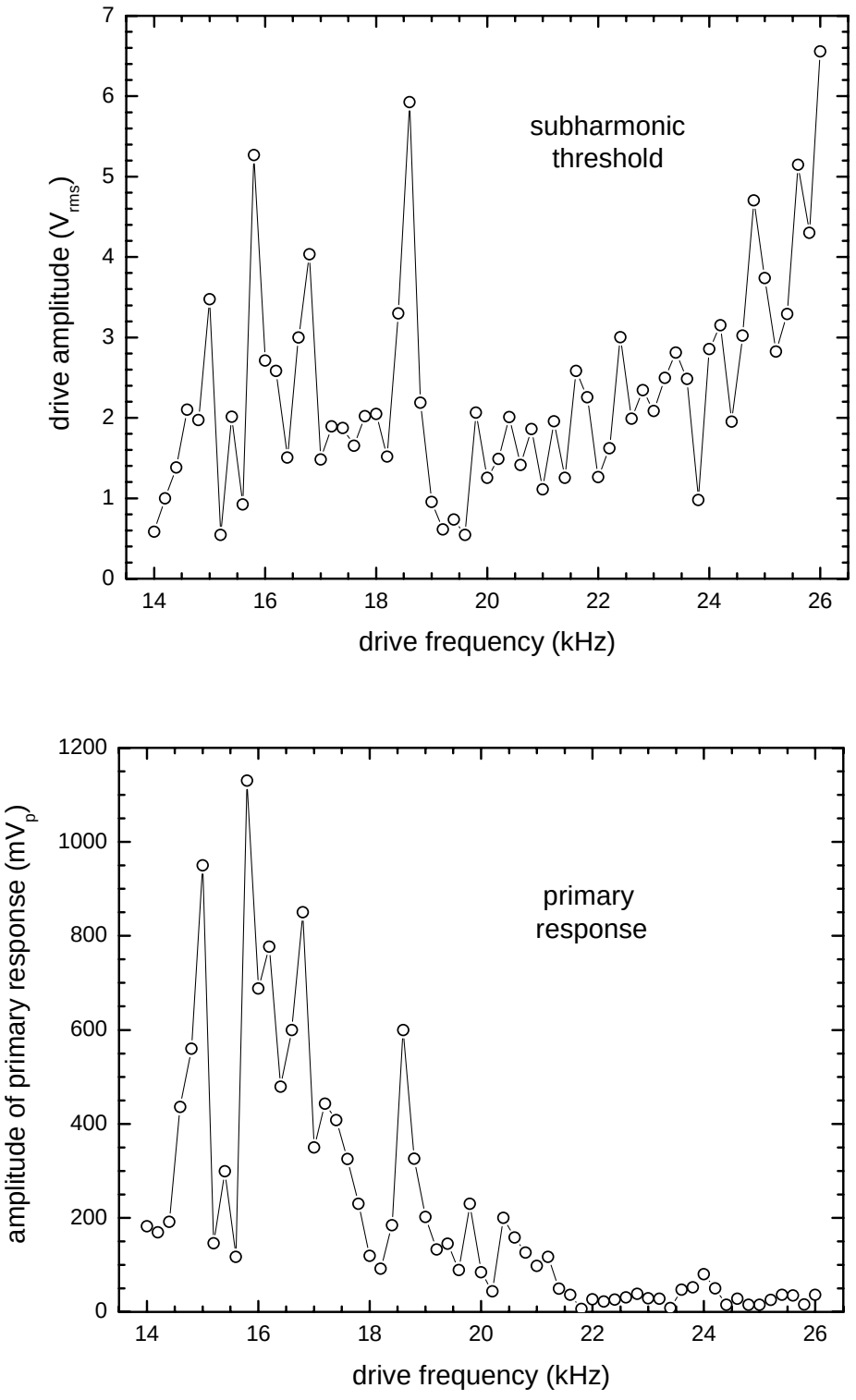

Figure 24. Threshold drive amplitude for subharmonic excitation as a function of drive frequency (top graph). The data points are connected by straight line segments as a guide to display the variation of the values. The bottom graph is the corresponding amplitude of the primary response (at the frequency of the drive).

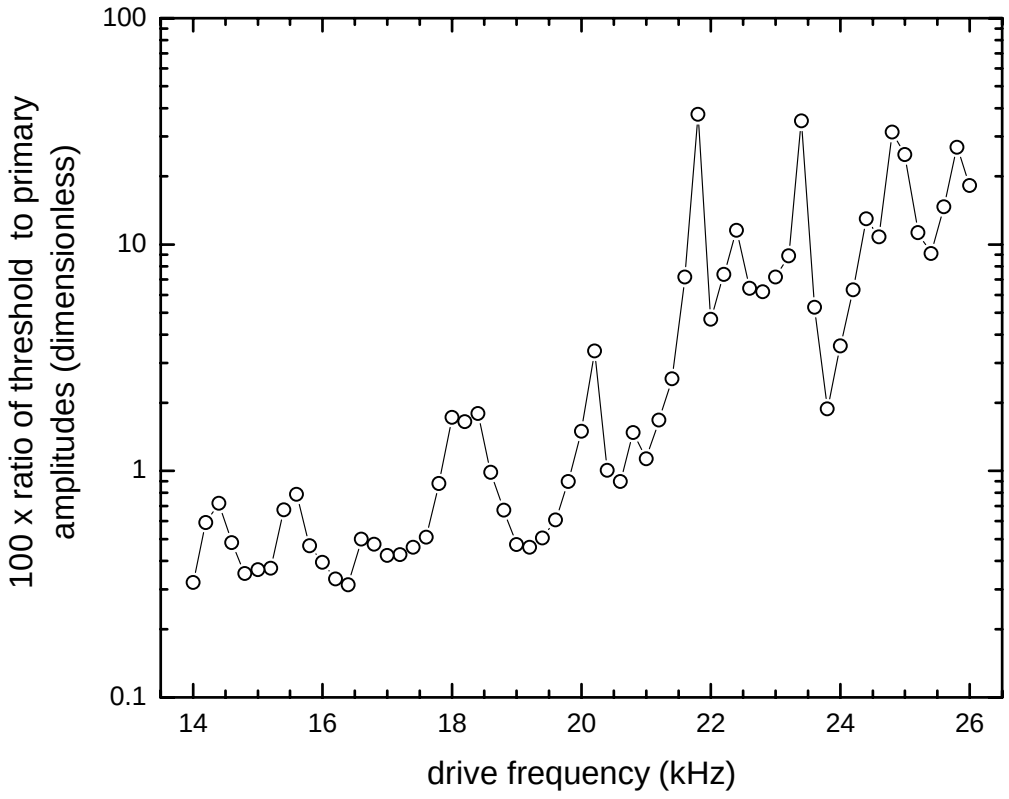

Figure 25. Subharmonic threshold drive amplitude normalized to the amplitude of the primary response. A logarithmic ordinate is used so that the variation of all of the data can be clearly discerned. Each trough suggests parametric excitation of a different mode.

It should be noted that there is a means of maintaining a primary response with an approximately constant amplitude as the frequency is changed. This method is to use a constant current source rather than the standard constant voltage source, which we used due to convenience.

Finally, some general comments must be made regarding our experimental investigations of the nonlinear behavior of a compression driver: (i) we observed many more nonlinear phenomena than reported above, and (ii) our

investigations were often seriously hampered by a lack of reproducibility of the data. Our experience was confined to the JBL 2450 model, but this behavior is probably common to all compression drivers, and may extend to cone loudspeakers.

In regard to (i), the appearance of unexpected phenomena is typical in experimental investigations of nonlinear systems, which tend to be overwhelmingly rich in behavior. As an example in our system, at a drive frequency of 3.0 kHz we clearly observed f/3, which, as far as we know, cannot be explained as parametric excitation. At other frequencies, we also occasionally did not observe f/2 but, rather, two sidebands equally-spaced about f/2. This behavior may have been due to a nonlinear coupling to some lower-frequency mode. As another example of interesting nonlinear behavior, consider the subharmonic response amplitude as a function of drive amplitude (Figure 23). At greater drive amplitudes (beyond the graph), there can a substantial range in which the response amplitude *decreases* with increasing drive amplitude. In other cases, quasiperiodicity develops.

In regard to (ii), the use of drive amplitudes that are not small evidently causes temporary or permanent alteration of some parameters of a compression driver. However, the character of the data was almost always reproducible. One exception was the presence of f/3, which is mentioned above. On the days following this observation, we were unable to reproduce the result, even though we carefully searched at different frequencies.

D. SURVEY OF LITERATURE AND INTERPRETATION OF DATA

The experimental evidence in previous section (Sec. C) suggests that the generation of f/2 subharmonics in a compression driver is due to parametric excitation of a mode. Moreover, for different drive frequencies, different modes are excited. The evidence is the abrupt appearance of a subharmonic as the drive amplitude is slowly increased, and a threshold drive amplitude that exhibits a sequence of minima as the drive frequency is varied.

To try to determine whether this conclusion is correct and, if so, what modes are being parametrically excited, we decided to search the scientific literature. We initiated the search by contacting JBL Professional Corporation, and we were fortunately led to Dr. Alex Voishvillo, who is an expert on the nonlinear dynamics of compression drivers. He graciously sent us many current technical papers on the subject, and these papers led us to other scientific literature. We were surprised to find that subharmonic generation in compression drivers is an active area of research in the audio engineering industry. The goal is to understand the behavior in order to reduce its occurrence. We repeatedly encountered the statement in the literature that loudspeakers and compression drivers are the weakest link in sound reproduction and sound reinforcement. The following are synopses of the relevant literature, in chronological order:

● Pedersen (1935) comments that a discrete spectrum of f/2 subharmonics was observed in a loudspeaker (with a cone rather than a diaphragm), and that the amplitude of a subharmonic rises very quickly with drive amplitude above a threshold. However, because few investigators at that time believed in the existence of subharmonics, Pederson devotes nearly all of the lengthy paper to dealing theoretically with parametric excitation of a single-degree-of-freedom system. Pedersen (1935b) presents detailed comparisons of theory and experiment for few-degree-of-freedom mechanical and electrical systems. No contact is made with loudspeakers.

● Olson (1947, 1957) comments that f/2 subharmonic generation is well known in loudspeakers and is very pronounced in the mid-frequency range. As a model equation, he uses a damped driven oscillator with a cubic nonlinearity in the force (which is now referred to as a type of Duffing equation). Olson claims to have obtained solutions that have subharmonics. This is a very surprising claim because, to our knowledge, a cubic nonlinearity cannot give rise to parametric excitation at f/2. However, the equation can yield chaos, and might possess a period-doubling route to chaos, similar to a driven pendulum (which also has an antisymmetric nonlinearity). If Olson observed period-doubling, this would have been decades ahead of its discovery in the 1970s!

Figure 26 is a sketch from Olson's book which shows one mechanism of parametric excitation of a cone mode. This excitation causes sound to be radiated at half the drive frequency. This type of parametric excitation is similar to length modulation of a string under tension, which has been known since the mid-1800s to yield excitation at half the drive frequency.

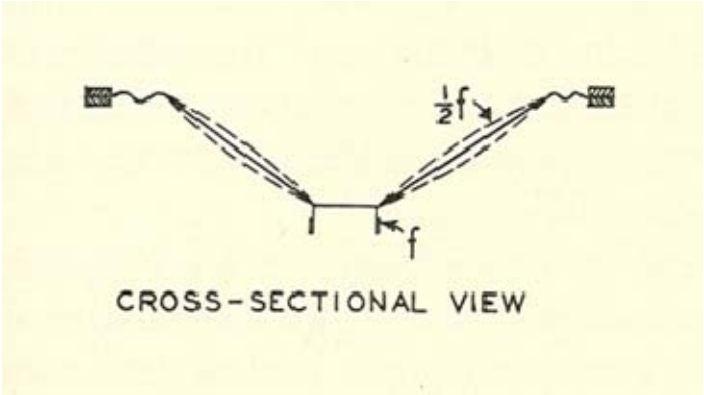

Figure 26. Parametric excitation of a cone mode of a loudspeaker, from Olson (1947, 1957). The frequency of the mode is half the frequency at which the voice coil is driven.

Finally, Olson states that the smallness and stiffness of the diaphragms of compression drivers are unfavorable for the production of subharmonics. We might conclude from this statement that later manufacturing advances reduced the diaphragm thickness and thus the mass, in order to increase the amplitude of the radiated sound, and also increased the diameter in order to increase the amplitude of the radiated sound. Indeed, the JBL 2450 has a titanium diaphragm of diameter 4 inches and thickness 0.002 inch.

● Cunningham (1951) considers a loudspeaker, and restricts the investigations to a drive frequency that is twice the resonance frequency of the loudspeaker. Excitation at the resonance frequency is achieved, and is assumed to be parametric excitation, although this is not proved. In sound reproduction cases in which the amplitudes and phases at different frequencies are continually changing, Cunningham argues that the growth rate of the subharmonic is typically too slow to have a deleterious effect.

● Hubbard (1988) performed experiments that yielded f/2 subharmonics in various compression drivers, and confirmed the results with a current source (rather than a voltage source). The data reveal a multitude of f/2 subharmonics at discrete frequencies. Citing Olson (1947, 1957) Hubbard speculates that the subharmonics may be due to a vibrational mode of the diaphragm or the nonlinearity of the suspension. He suggests that mathematical calculations be done, and that laser imaging techniques be employed to observe the motion of the diaphragm.

● The paper of Aldoshina, et al. (1998) is very difficult to understand, because the English is extremely poor and because the scientific presentation is substandard. The investigation is of loudspeakers. (The word “diaphragm”

should be replaced with “cone.”) The authors claim that an f/2 subharmonic is due to parametric excitation of a vibrational mode, and claim that theoretical calculations are in approximate agreement with experimental measurements.

● A follow-on paper of Aldoshina, et al. (1999) is much better than the previous paper. A comparison of theory and experiment appears to allow no doubt that subharmonic generation at frequencies other than the fundamental mode of cone driver is due to parametric excitation of a deformation mode of the cone, and that different deformation modes can be excited depending upon the drive parameters. The parametric drive arises due to nonlinear coupling of the primary response and deformation modes of the cone.

● Voishvillo (2003, 2004) gives an extensive theoretical treatment of nonlinear effects in compression drivers, although the possibility of parametric excitation is not addressed. The theory only applies at mid-range frequencies (roughly 500 Hz to 5 kHz), and the dome is thus treated as rigid. However, one interesting effect that is considered is the parametric modulation of the stiffness and mass of the air in the compression chamber. This modulation is due to the change in volume caused by the displacement of the dome. We comment further on this below.

● Bolaños (2005) performed experiments with four different compression drivers, only two of which exhibited f/2 subharmonic generation over the range of roughly f = 12 – 20 kHz. One of these drivers has a subharmonic response at only one frequency (f/2 = 8.48 kHz), and the other driver at two frequencies (f/2 = 7.80, 8.54 kHz). Bolaños gives results of numerical simulations of the deformation modes of a diaphragm, and emphasizes that these modes involve the whole moving assembly (including the voice coil and the suspension). He gives qualitative arguments of how these modes can be parametrically excited by the primary response. No quantitative connection with the compression drivers in the experiment is made.

The above synopses show that the understanding of subharmonic generation in compression drivers has recently progressed rapidly, although further investigations are needed. At this point, however, it appears to be nearly certain that the subharmonics are due to the primary response at a high frequency f parametrically driving a deformation mode of the diaphragm assembly at frequency f/2, due to nonlinear coupling of the primary response and the deformation modes. Bolaños's (2005) drivers yield parametric excitation of very few diaphragm modes, whereas our driver yields a multitude. This contrast initially concerned us, because we thought that the behavior in our driver might be due to a fundamentally different effect. It should be noted that Hubbard (1988) also observed a multitude of modes. It is clear from the literature that the behavior of different compression drivers can vary substantially. Our data is completely consistent with parametric excitation of diaphragm modes, and so there is no reason at this point to suspect that any phenomenon other than parametric excitation is occurring.

Finally, the above work of Voishvillo (2003) regarding the modulation of the air stiffness and mass in the compression chamber prompted us to consider the interesting possibility that the fundamental ("mass-on-a-spring") mode of the compression driver could be parametrically excited as a result of the modulation. As stated in Sec. C, we had observed f/2 subharmonic generation at a drive frequency of f = 1.0 kHz. Could this be parametric excitation of the fundamental mode of the compression driver? In a quick and crude experiment, we found that the threshold drive amplitude to excite the subharmonic indeed has a minimum, and that this occurs at f = 1.4 kHz, where the drive amplitude is about 3.0 V_{rms}. If the fundamental mode is being parametrically excited, the resonance frequency of the driver should then be half of about 1.4 kHz, or 700 Hz. It was only after this prediction that we checked the specifications sheet of the JBL 2450 model. When the driver is connected to a standard horn, which is roughly similar to our situation with no horn, the resonance frequency is 650 Hz. (When the driver is connected to a pipe, the resonance frequency is 500 Hz.) We conclude that the

f/2 subharmonic excitation for drive frequencies in the approximate range f = 1-2 kHz is due to parametric excitation of the fundamental mode of the driver. We have not found any mention of this in the literature.

The results of this chapter are schematically summarized in Figure 27. We have shown that a compression driver offers a dramatic demonstration of parametric excitation when driven at a high frequency (roughly 20 kHz), and that deformation modes of the diaphragm assembly are being excited. At low frequency (1-2 kHz), parametric excitation of the fundamental mode of the driver occurs. This low-frequency excitation suffers as a lecture demonstration because the sound level of the response at the drive frequency is so high that the audience would require some type of hearing protection. However, firmly seating a finger in each ear may be sufficient.

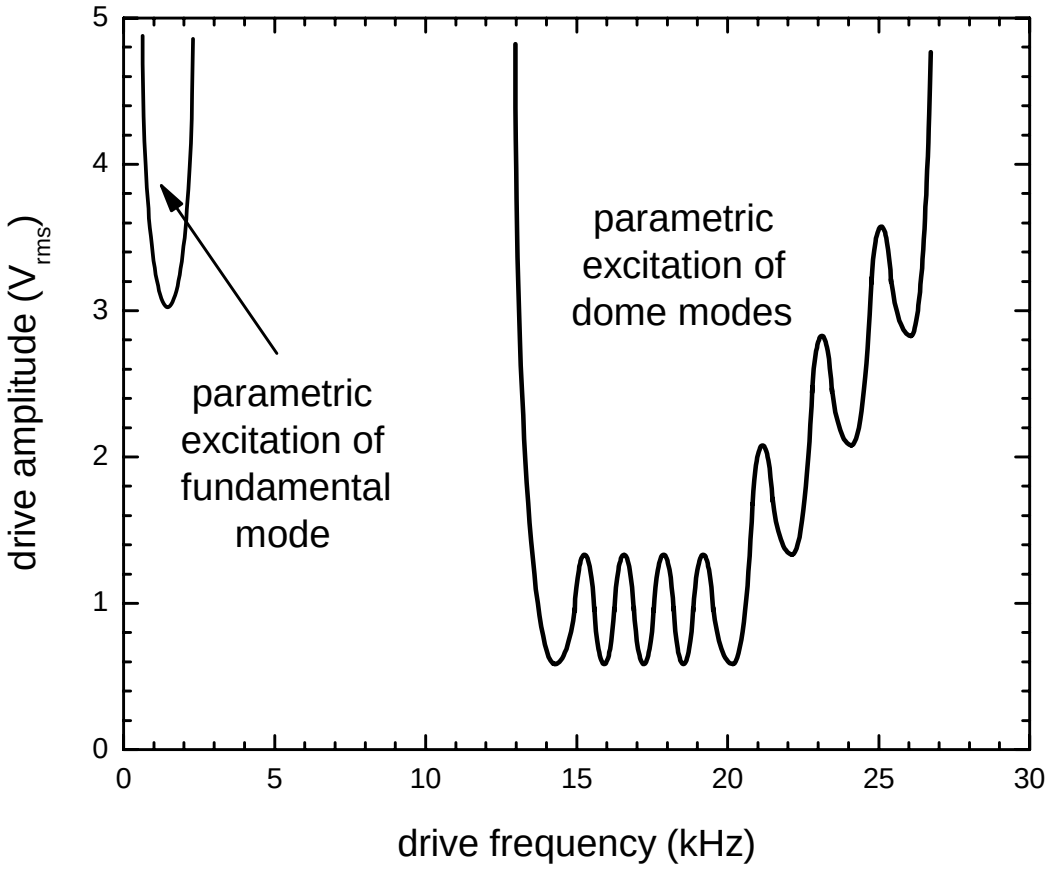

Figure 27. Schematic representation of the rough drive parameter regions over which parametric excitation occurs in a compression driver. The frequency of the excitation is half the drive frequency.

V. PARAMETRIC EXCITATION OF A TORSIONAL OSCILLATOR

In this chapter, we discuss the background and improvements made to a parametrically excitated torsional oscillator apparatus in which the length of the oscillator is modulated. The background and reasons for this work are stated in Sec. A, the improvements are detailed in Sec. B, the demonstration of the apparatus is described in Sec. C, and any future work that could be performed will be presented in Sec. D.

A. BACKGROUND

In the spring of 2005, an investigation into the parametric excitation of a torsional oscillator was conducted by Ensign Michael Janssen. The oscillator consists of a strip of material with a rod attached to the lower end (Figure 28), so that torsional oscillations can occur. Near the top of the strip is a double-roller that sandwiches the strip. A motor causes the double-roller to oscillate up and down, modulating the length and thus the frequency of the torsional oscillatior. We will take a look at the construction of the apparatus which was developed in Janssen's thesis. It is necessary to understand the background and the fundamental workings of the apparatus in order to understand the improvements that were undertaken.

As developed in Ensign Janssen's thesis, we will visit the original construction of his apparatus, and then in Sec. B we will see how I improved the original apparatus to make it a feasible classroom demonstration. Ensign Janssen implemented his work in three phases. Phase one consisted of constructing the support structure. This task included the design and making of the frame, the three leg leveling system, and the acrylic mounting for the motor. The next phase consisted of constructing the roller guide and ribbon clamp. Two rollers were machined to be as identical as possible so that there would not be any nonuniformities in the rolling mechanism. The final phase of construction

involved creating the drive system. The drive system used in the original construction consisted of a salvaged motor that no specifications were known and a 60 to 1 ratio gear box which was also salvage from another piece of equipment. This was done because of the timing issue with his thesis. Ensign Janssen's end product can be seen in Figure 28. The ground work for the apparatus was laid out, but there were several improvements that needed to be made to his work, and I will address these as they occurred in my work in Section B.

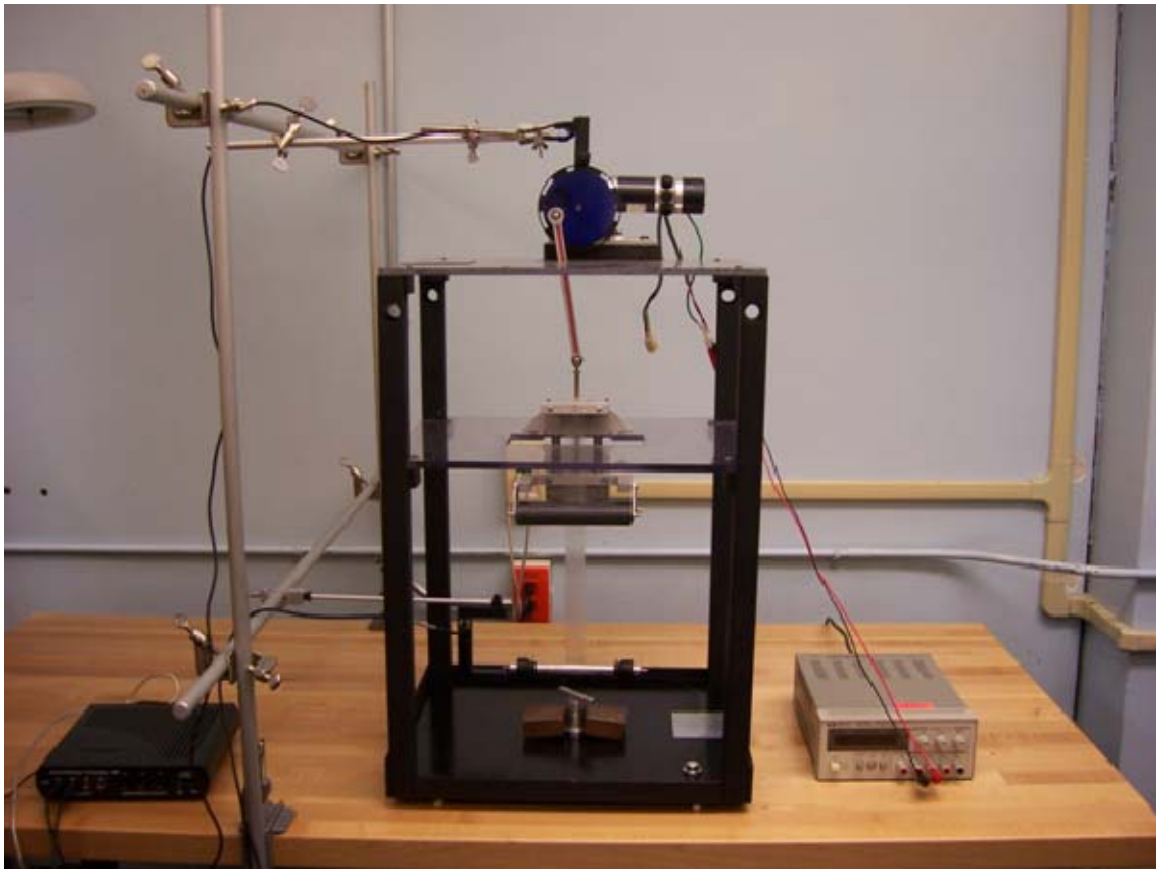

Figure 28. Original torsional oscillator.

B. IMPROVEMENTS

There were several improvements that were needed to make the apparatus a feasible demonstration for the classroom. The improvements were made in various steps. The first step was to find a strip with a higher stiffness

than that used in previous work so that the restoring force would be much greater. The second step was to find a motor that fit the parameters of the new material and possibly be used if even further improvements are made. The third improvement was to maintain the integrity of the design to meet the new specifications of the motor and strip.

Step one of this process was done by measuring the natural frequency of several individual strips. Since each strip had a different natural frequency, thickness, and color, we will reference them by the color. There were four strips measured which gave a span of different frequencies to run the motor. To measure the natural frequency of each strip, I attached the strip to the apparatus and displaced the oscillator with my hand. As the oscillations decayed the natural frequency was measured over a time of thirty seconds. I counted the number of oscillations in that given time and calculated the period and then converted these measurements to a frequency and RPM. The strip used in previous work had a natural frequency f=.132 Hz and had to be driven at .264 Hz or 15.84 RPM. The natural frequencies and driving RPM to excite each strip are shown in Table 1.

Strip	Period	Natural Frequency (Hz)	RPM(for Twice NF)
Pink	1.38	0.72	86.71
Orange	1.34	0.74	89.22
Yellow	0.99	1.00	120.48
White	0.74	1.36	163.04

Table 1. Natural frequencies and drive RPM to parametrically excite each strip.

Each new strip could not be used on the previous apparatus due to the motor. The motor used in the construction of the first apparatus did not have any specifications, but was known not to provide enough torque to parametrically excite a strip with a frequency higher than .132 Hz. The new motor would have

to provide a much higher torque and variable RPM speeds to be effective at the parametric excitation of this oscillator.

The new motor shown in Figure 29 was attached to the top of the apparatus on an acrylic mount. It is a Bodine model 3399, 3/8 Horsepower, DC brushless motor with a built in gearbox with a ratio of 10:1. Without the gearbox the motor had a max RPM speed of 2500 RPM, and once the gearbox was attached it had a max speed of 250 RPM and a minimum speed of 20 RPM. Since the stiffest strip that is in the inventory has to be driven at 163 RPM this motor more than exceeds the needed RPM speeds. We wanted to use this apparatus as a classroom demonstration, and with the new motor, it has cut down on the excitation time dramatically.

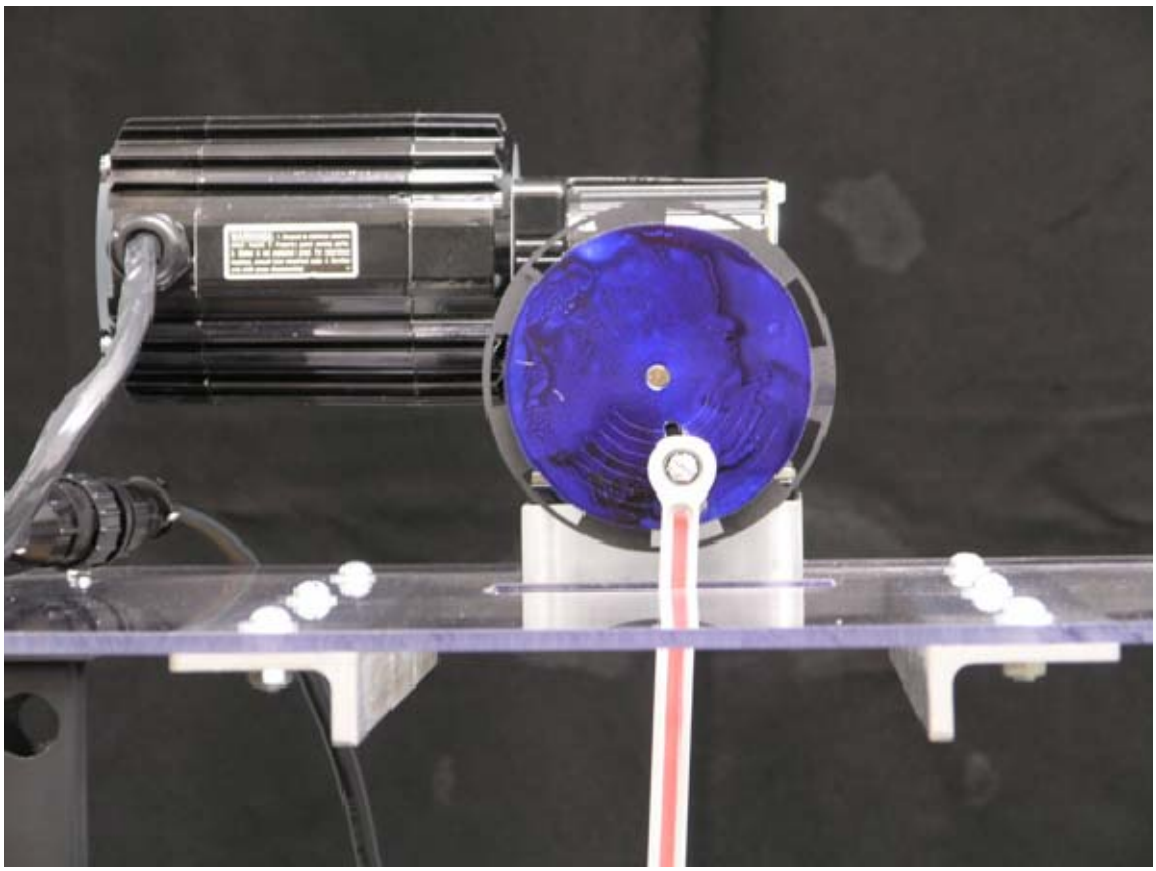

Figure 29. New motor.

The other features in which this motor offered was that it required a controller. With the controller shown in Figure 30, the ability to operate the motor at variable RPM speeds was now a possibility. This feature was a large improvement over the previous motor, but the dial on the new controller was not enough to give a precise RPM readout. Bodine also made a tachometer which could hook up to the controller. With this feature the demonstrator would be able to dial up a precise RPM necessary to parametrically excite the oscillator. This feature was very important because it allowed the demonstrator a quick transition from the discussion to the demonstration. If the tachometer had not been added on then the demonstrator would have to search for the right speed which could take away from the demonstration itself.

Figure 30. Controller box setup for tachometer output.

The point came where the construction of the apparatus had to be modified due to the new parts. Since the motor was much larger than the previous, the motor had to be mounted on a 1 inch thick piece of acrylic, and the motor platform had to be extended a couple of inches to allow the original frame to still be used. The new motor also provided a much greater torque. Due to the increased amount of torque the top plate of acrylic in which the motor was mounted was flexing. The effects of this were causing the entire apparatus to shake and go off balance. The first remedy to this problem was to install aluminum bracing to the top plate to try and secure the flexing response of the system. This did stop the flexing of the top plate for the most part, but it did not stop the entire system from rocking due to the original design of three legs. The previous motor was operated at such low speed that it did not cause to system to rock at all, so it was built with three base legs so that it would be easier to level. The previous leveling system, however, was a problem given the speed and the amount of torque at which the new motor operates. Two base aluminum plates were added giving the apparatus four base legs instead of three. With this improvement the apparatus was almost completely stable and the end product can be seen in Figure 31. Further improvements to the structure of the frame will be discussed in Sec. D for future work.

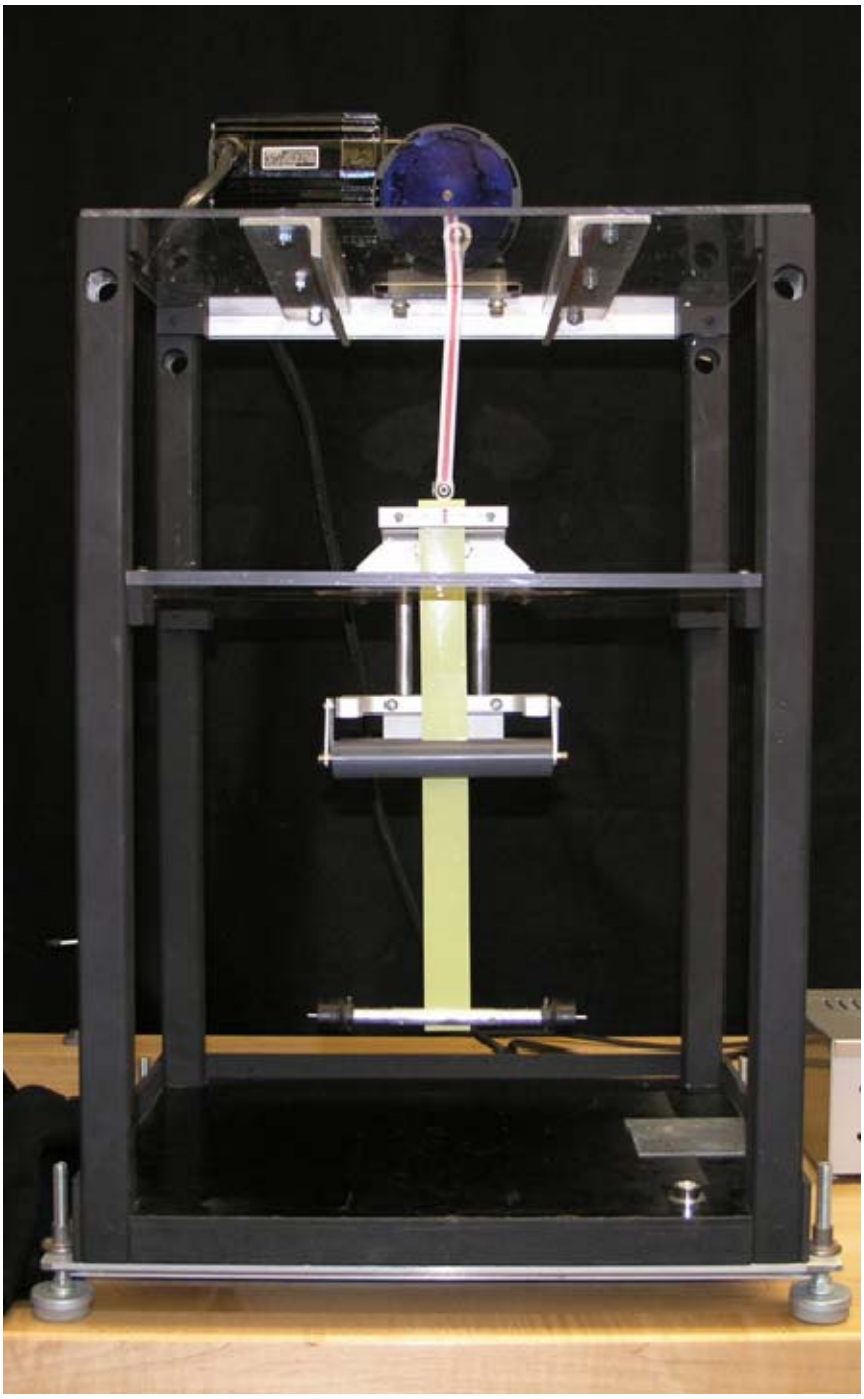

Figure 31. Modified version of the parametrically excited torsional oscillator apparatus.

The next problem faced was that due to the increased stiffness of the strip being used. The rollers were not able apply the proper tension needed to keep the strip in place; the strip was causing the rollers to spread and shake due to the tension problem. This problem caused the pendulum motion of the strip to be excited which damped out and took over the torsional effect. The quick remedy to this was to install springs to each side of the rollers to try and fix the problem. This can be seen in Figure 32. Once the springs were in place to pendulum motion was not excited as easily. This can sometimes occur at very high RPM speeds, but further improvements to the roller mechanism will be discussed in Sec. D for future work.

Figure 32. Rollers with new tension spring.

C. DEMONSTRATION

This apparatus was created for the purpose of showing the parametric excitation of a torsional oscillator. The demonstrator will select the yellow strip in Table 1, and will then set the dial to the proper RPM speed. The yellow strip was selected due to its high stiffness. If one of the stiffer strips are chosen then the total displacement of the oscillator decreases causing less of a visual effect. Once the proper drive frequency is set then the motor will be started via the controller. The motor then drives a locomotive type arm, and the rollers roll up and down a strip of some stiffness. This causes the length modulation of the apparatus which in turn parametrically excites the torsional oscillations of the system. For most of the strips, it takes about 30 seconds for the apparatus to become parametrically excited, so the lecturer should start the demonstration and lecture concurrently.

D. FUTURE WORK

The apparatus is ready for lecture demonstrations. Any future work would be for the purpose of research or to make the demonstration even more efficient. The areas which could be improved upon consist of the structure of the apparatus and the material used for the strip. The structure has been vastly improved, but the way in which the apparatus is driven it has metal on metal rubbing. We would like see roller bearing inserted into the driving components. This would allow for much smoother stroke, and would decrease the amount of lubrication in which the apparatus requires. The next improvement would be to purchase a different material for the strip. We would like a material that the stiffness was known. With a better material that was cut properly the system would look much cleaner.

THIS PAGE INTENTIONALLY LEFT BLANK

VI. CONCLUSIONS

Nonlinear oscillations and waves are an important area of educational study. Due to the difficulty of the subject matter it is vital to have classroom demonstrations. We have paved the path for future thesis students to take the initial development our nonlinear gravity wave demonstration and create a feasible classroom demonstration. We have shown that subharmonic generation due to parametric excitation in a compression driver is a feasible demonstration. The torsional oscillator demonstration has now been drastically improved and is classroom ready. The nonlinear capillary wave demonstration was a failed project, but it will allow insight into possibilities that may work for future attempts. This thesis was designed for the express purpose of developing demonstrations and furthering research into the subject of nonlinearity. We have accomplished both goals, and have made several developments that allow for continued research and give better understanding to the students to take courses involving nonlinearity.

THIS PAGE INTENTIONALLY LEFT BLANK

LIST OF REFERENCES

Analog Devices. *Balanced Modulator/Demodulator AD630*. Norwood, 2004.

Aldoshina, I., Bukashkina, O., and Tovstik, P., *An Advanced Model of Nonlinear Parametric Vibrations of Electrodynamical Loudspeaker Diaphragm*, 106th Aud. Eng. Soc. Convention, Munich, May 1999.

Aldoshina, I., Bukashkina, O., and Tovstik, P., *Theoretical and Experimental Analysis of Nonlinear Parametric Vibrations of Electrodynamical Loudspeaker Diaphragm*, 104th Aud. Eng. Soc. Convention, Amsterdam, May 1998.

Bolaños, F., *Measurement and Analysis of Subharmonics and Other Distortions in Compression Drivers*, 118th Aud. Eng. Soc. Convention, Barcelona, May 2005.

Burr-Brown Corp. *Fast-Setting FET-Input Instrumentation Amplifier*. Tucson, 1986.

Cunningham, W. J., *The Growth of Subharmonic Oscillations*, J. Acoust. Soc. Am. **23**, 418-422 (1951).

Denardo, B., and Larraza, A., *Nonlinear Oscillations and Waves: An Essential Introduction with Demonstrations* (Naval Postgraduate School, Department of Physics, 2004). This text is used for the NPS course PH4459 (Nonlinear Oscillations and Waves).

Denardo, B., Earwood, J., and Sazonova, V., *Parametric instability of two coupled nonlinear oscillators*, Am. J. Phys. **67**, 187-195 (1999).

Fairchild Semiconductor. *Low Power Monostable/Astable Multivibrator*. May 1999.

Hubbard, J. K., *Subharmonic and Nonharmonic Distortions Generated by High Frequency Compression Drivers*, 6th Aud. Eng. Soc. Convention, May 1988.

Janssen, M., "Investigations of Parametric Excitation in Physical Systems," M.S. thesis, Department of Physics, Naval Postgraduate School, June 2005.

Landau, L. D., and Lifshitz, E. M., *Fluid Mechanics* (Pergamon, New York, 1959), pp. 39 and 282.

Mandelstam L., Papalexi N., Andronov A., Chaikin S., and Witt A., “Report on Recent Research on Nonlinear Oscillations” NASA Technical Translation, NASA TT F-12, 678. November 1969.

Pedersen, P. O., *Subharmonics in Forced Oscillations in Dissipative Systems, Part I*, J. Acoust. Soc. Am. **6**, 227-238 (1935a).

Pedersen, P. O., *Subharmonics in Forced Oscillations in Dissipative Systems Part II,* J. Acoust. Soc. Am. **7**, 64-70 (1935b).

Smith, D., “Parametric Excitation of an Acoustic Standing Wave,” M.S. thesis, Department of Physics, Naval Postgraduate School, June 2003.

Varnadore, P., “Feasibility Investigations of Parametric Excitation of Acoustic Resonators,” M.S. thesis, Department of Physics, Naval Postgraduate School, June 2001.

Voishvillo, A., *Nonlinear versus Parametric Effects in Compression Drivers*, 115th Aud. Eng. Soc. Convention, New York, October 2003.

Whitham, G. B., *Linear and Nonlinear Waves* (Wiley, New York, 1974), p. 475, 561.

INITIAL DISTRIBUTION LIST

1. Defense Technical Information Center
   Ft. Belvoir, Virginia

2. Dudley Knox Library
   Naval Postgraduate School
   Monterey, California

3. Physics Department
   Naval Postgraduate School
   Monterey, California

4. Professor Bruce Denardo
   Department of Physics
   Naval Postgraduate School
   Monterey, California

5. Professor Thomas Hofler
   Department of Physics
   Naval Postgraduate School
   Monterey, California

6. James Luscombe
   Chair, Physics Academic Committee
   Naval Postgraduate School
   Monterey, California